Silicon nanoparticles: applications in cell biology and medicine

Norah O'Farrell
Andrew Houlton
Benjamin R Horrocks

School of Natural Sciences,
University of Newcastle upon Tyne,
UK

Abstract: In this review, we describe the synthesis, physical properties, surface functionalization, and biological applications of silicon nanoparticles (also known as quantum dots). We compare them against current technologies, such as fluorescent organic dyes and heavy metal chalcogenide-based quantum dots. In particular, we examine the many different methods that can be used to both create and modify these nanoparticles and the advantages they may have over current technologies that have stimulated research into designing silicon nanoparticles for in vitro and in vivo applications.

Keywords: biology, medicine, nanoparticles, quantum dots, silicon

Introduction

Fluorescent labeling is a technique that allows the investigation of both cell structure and function. It is widely used in immunofluorescence applications. Immunofluorescence techniques involve staining cells with antibodies that have been conjugated to fluorescent dyes, such as fluorescein and phycoerythrin. This method is often used to label molecules on the cell surface, but antibodies can also be directed at targets in the cytoplasm. In addition to specific labels, probes capable of responding to the physiological state of a cell, eg, membrane potential or the internal ion concentrations have also been developed. Furthermore, fluorescent molecules that can change their optical properties in response to changes in a particular aspect of their environment have also been developed. For example, the dye Indo-1 exhibits a spectral shift in its emission on binding calcium ions. Molecules such as these are known as indicator molecules, as they may be used to monitor the concentration of the molecule to which they are sensitized. Fluorescent indicators currently exist for calcium, pH, ATP, membrane potential, and some neurotransmitters (Invitrogen 2005). However, if the aim is to observe/monitor changes in living specimens, then there are serious limitations with standard fluorescence techniques (see below for further discussion of these limitations). Quantum dots have the potential to overcome these difficulties; therefore this new technology continues to develop rapidly.

Quantum dots

The luminescence characteristics of molecular dyes and quantum dots are a consequence of their electronic structure (Figure 1). Whilst molecules have a discrete energy level spectrum and solids have continuous bands of energy levels, nanoparticles are intermediate and can be viewed either as large molecules or small pieces of the solid. The color of luminescence from these systems depends on the energy gap between the highest occupied molecular orbital and the lowest unoccupied molecular orbital. In equivalent solid state terminology, the bandgap is the difference between the

Correspondence: Norah O'Farrell
School of Natural Sciences,
Bedson Building, University of
Newcastle upon Tyne, NE1 7RU, UK
Tel +44 191 222 5402
Fax +44 191 222 6929
Email norah_ofarrell@hsa.ie

451
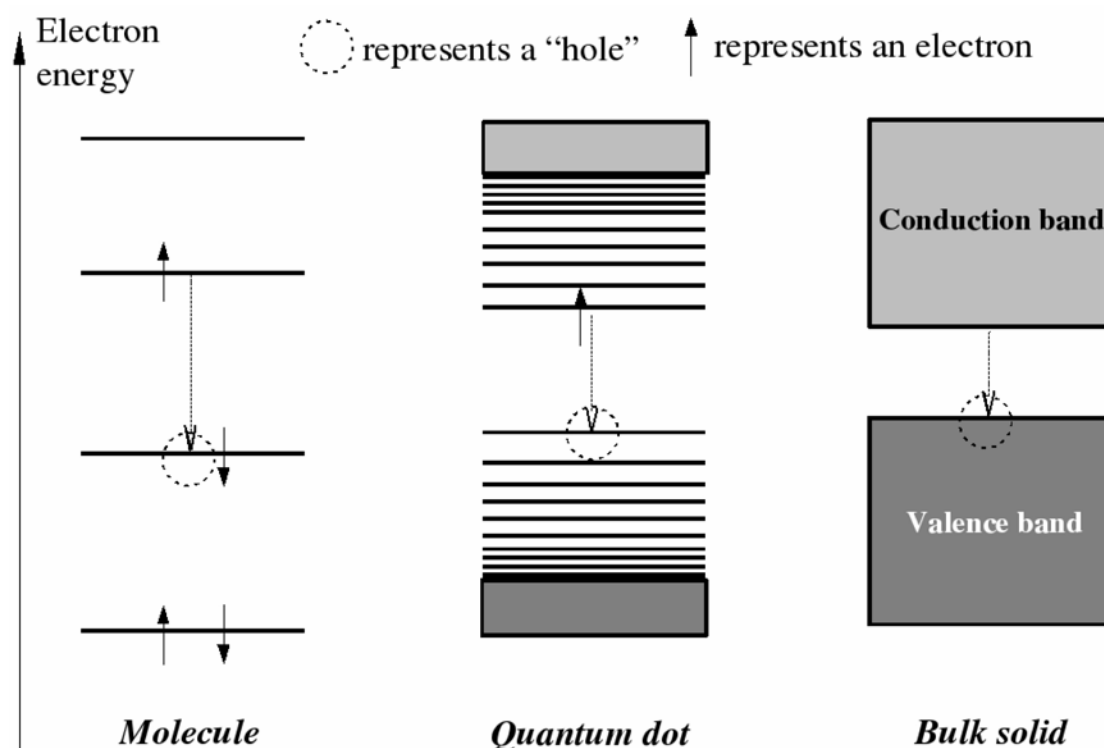
Figure 1 Schematic energy level structure of (left) molecular dyes, (center) quantum dots and (right) bulk semiconductor. The dotted arrow indicates the electronic transition responsible for the luminescence.

top of the valence band and the bottom of the conduction band[1]. Nanoparticles in the size range where the electronic properties are changing between solid-like and molecular have luminescence characteristics strongly dependent on their size. These particles are commonly known as quantum dots because the size-dependent changes in electronic structure are related to the constraint imposed on the electron wavefunctions by the surface as the particle radius decreases – an effect known as quantum confinement.

In general, small particles of semiconductor show large size-dependent changes in their spectroscopy below a radius of a few nm; the precise radius is characteristic of the material: these quantum confinement effects set in for particle radii of 5 nm for silicon (Si) and for cadmium selenide (CdSe), a widely employed luminescent label. This behavior is sketched in Figure 2. Absorption of light in the bulk semiconductor promotes an electron to a higher energy orbital and creates an unoccupied orbital at lower energy (a "hole") which behaves as a mobile positive charge. The lowest excited state of the solid can be pictured as consisting

of the electron orbiting the hole in a manner analogous to the hydrogen atom. However, compared with the hydrogen atom, there are two important differences: the effective mass of the hole is much less than that of the proton and the electrostatic interaction between the electron and hole is screened by the intervening atoms in the solid. The radius of the wavefunction describing the electron-hole pair (exciton) is therefore much
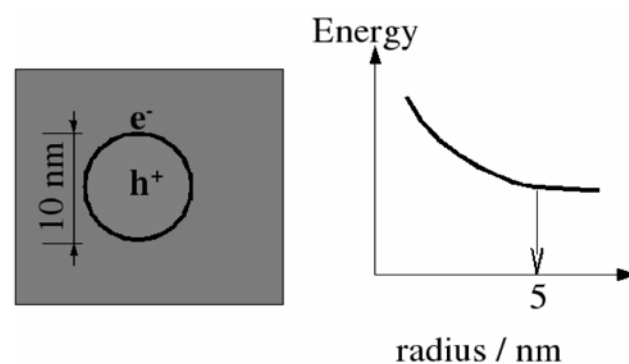
Figure 2 Radius of an excited state produced by absorption of light in a particle of semiconductor (left) and the variation of the energy with the particle radius (right).

---

[1] Bandgaps can be classified as either direct or indirect, depending on the band structure. A direct bandgap means that the conduction band lies directly above the valence band on a plot of energy against electron wavevector. An indirect bandgap means that the bottom of the conduction band is shifted relative to the top of the valence band. The main consequence of this is the emission and absorption of light corresponding to the movement of an electron across the gap is "dipole forbidden" and therefore weak. It should be noted that this terminology relates to bulk materials, but the behavior of nanoparticles of direct gap materials, eg, CdSe, is markedly different to that of nanoparticles of indirect gap materials, eg Si.

larger (5 nm) than the Bohr radius of hydrogen (0.053 nm). Clearly this picture has to change when the particle radius itself is less than 5 nm and so the radius of the exciton defines the size below which strong confinement effects set in. In the simplest models, the energy of the photon emitted when the electron and hole recombine is:

$$hv = E_g + \frac{\hbar^2\pi^2}{2R^2}\left(\frac{1}{m_e} + \frac{1}{m_h}\right)$$

where E_g is the bulk bandgap, R the particle radius, and m_e and m_h are the effective masses of the electron and hole.

## Quantum dots as luminescent labels
Difficulties associated with conventional fluorescent dyes

Fluorescent labeling of biological materials is most commonly achieved with organic dyes, eg, rhodamine, fluorescein, phycoerythrin. These conventional fluorescent dyes have several well-documented shortcomings, such as narrow excitation wavelengths, broad emission spectra, typically with asymmetric, red-shifted spectral tails and concentration-dependent changes in luminescence efficiency due to self-quenching. However, low resistance to photodegradation is also a major problem (Invitrogen 2005). In confocal microscopy, the small aperture blocks almost all of the light emitted by the tissue under examination, therefore the exciting laser should be quite bright to allow an adequate signal-to-noise ratio. Such intense illumination however, causes the dyes to fade within minutes of continuous scanning. In addition to photobleaching, phototoxicity is also a problem as excited fluorescent dye molecules can generate toxic free-radicals. Therefore, either the light intensity or the scan-time should be limited in order to prevent sample damage during imaging.

Advantages of quantum dots as luminescent labels in cell biology

Quantum dots possess several distinct advantages over their organic counterparts. Firstly, a narrow emission spectrum reduces spectral overlap. This increases the feasibility of distinguishing multiple fluorophores simultaneously. Secondly, the broad excitation spectrum of quantum dots facilitates the use of a single excitation wavelength to excite quantum dots of different colors. Thirdly, the large separation between the excitation and emission wavelength of quantum dots (the Stokes' shift) enables the whole emission spectra to be collected, resulting in improved sensitivity of detection (Jaiswal and Simon 2004) (see Figure 3).

Quantum dots are often brighter than conventional dyes due to the compounded effects of extinction coefficients that are an order of magnitude larger than those of most dyes, comparable quantum yield, and similar emission saturation levels (Michalet et al 2005). They are also not prone to variations in luminescence efficiency due to self-quenching. However, their main advantage resides in their resistance to bleaching over long periods of time (minutes to hours): this allows the acquisition of images that are both crisp and have high contrast. This increased photostability is particularly useful for three-dimensional (3D) optical sectioning, where bleaching of the fluorophores during acquisition of successive z-sections is a major issue (Michalet et al 2005). Some applications of quantum dots as multimodal contrast agents in bioimaging are summarized in Figure 4.
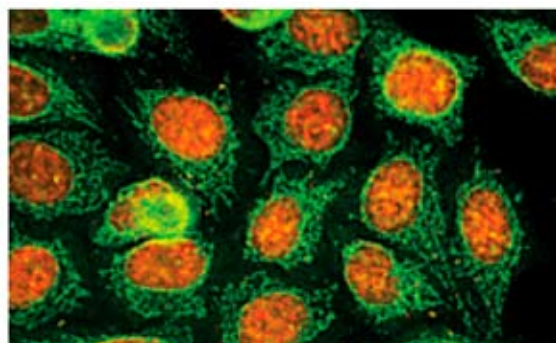
Figure 3 Double duty – green quantum dots cling to mitochondria in the cytoplasm; orange ones label proteins in the same cells' nuclei. Reproduced with kind permission of Prof. Sanford M Simon, Rockefeller University from Seydel C. 2003. *Science*, 300:80. Copyright © 2003 Sanford M Simon.
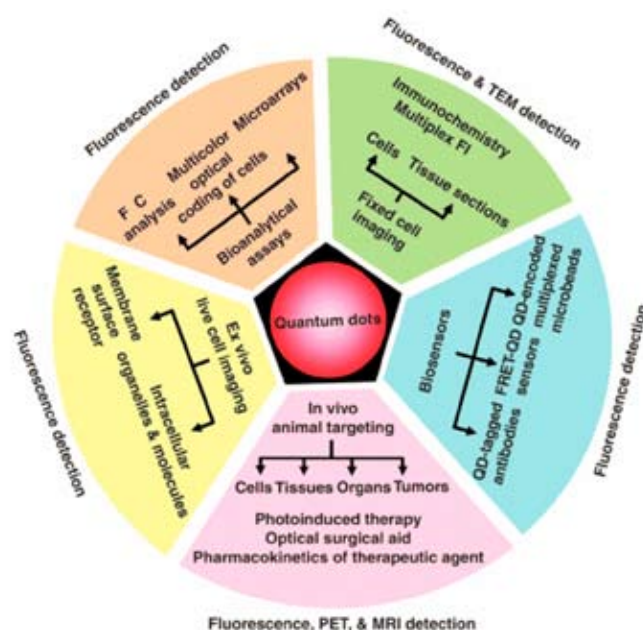
Figure 4 Applications of quantum dots as multimodal contrast agents in bioimaging. Reprinted with permission from Michalet X, Pinaud FF, Bentolila LA, et al. 2005. Quantum dots for live cells, in vivo imaging, and diagnostics. *Science*, 307:538-44. Copyright © 2005 AAAS.

Semiconductor quantum dots
Commercially available quantum dot probes

Two of the scientists responsible for many of the early studies on CdSe quantum dots and their properties, Moungi Bawendi and Paul Alivisatos went on to found the Quantum Dot Corporation (recently acquired by Invitrogen) and now a major supplier of quantum dots commercially. A growing range of conjugates and kits are available from the Quantum Dot Corporation including: Qdot® Western Blotting Kits for performing quantitative multiprotein analysis with stripping and reprobing; Qdot Streptavidin and Biotin Conjugates to label biotinylated proteins and DNA; Qdot Secondary Antibody Conjugates for performing multicolor labeling; Qdot Primary Conjugates; Qtracker® Cell Labeling Kits designed for facile labeling of live cells with Qdot nanocrystals; Qtracker non-targeted Quantum Dots for vascular and in vivo imaging; the Innovator Took Kit (ITK™) which provides chemical building blocks for assay development and optimization, and amino and carboxyl surface modification and Qdot Antibody Conjugation Kits which allow the consumer to conjugate their own antibodies to Qdot Nanocrystals.

Another company, Evident Technologies, founded in 2000 by Clinton Ballinger, Michael Locascio and Dan Landry commercialize their proprietary versions of quantum dots and sell them worldwide as EviDots™. They also incorporate EviDots into common plastics and polymers to create composites sold under the EviComposites™ brand name. For the life sciences market, Evident sell quantum dot-based fluorescent labels, under the EviTags™ (water stabilized quantum dots for biotechnology) and EviFluor™ (quantum dots fluors) names.

In December 2001, Nanoco Technologies was established in Manchester, UK to commercialize NanoDots™. Quantum dots for fluorescence labeling applications are often of the "core-shell" type; this means that the luminescent semiconductor nanocrystal (core) is coated with a higher bandgap material (shell). A common example is the CdSe core – ZnS shell nanoparticle. In this application, the shell isolates the core from the ambient chemical environment and mitigates corrosion of the core or quenching by adsorbates. The NanoDots produced by Nanoco include core, core-shell and Nanoco's new Ultrabright™ technology. The Ultrabright quantum dots vary in structure to the standard core or core-shell NanoDots and have the advantage of having a sharper emission and better optical efficiencies.

Applications of quantum dots

There are many detailed reviews on the uses of the CdSe/ZnS type of quantum dots for biological applications (Chan et al 2002; Parak et al 2003; Jaiswal and Simon 2004; Alivisatos et al 2005; Fu et al 2005; Michalet et al 2005; Parak et al 2005) and readers are directed to these for a fuller review of quantum dot applications. The type of studies where conventional heavy metal chalcogenide quantum dots have proved useful include: fluorescent labeling – Voura et al (2004), Dwarakanath et al (2004); conjugation – Dubertret et al (2002), Åkerman et al (2002), Wu et al (2003), Jaiswal et al (2003), Howarth et al (2005); and fluorescence resonance energy transfer (FRET) studies – Ebenstein et al (2004), Clapp et al (2004), Bakalova et al (2005). These studies illustrate both the potential and the limitations of current technology. Despite the success of the CdSe-based quantum dots as labels in biological experiments, there are some difficulties with the current technology. Concerns have been raised over the toxicity of the particles due to leaching of Cd^{2+} (Derfus et al 2004; Kirchner et al 2005) or the generation of reactive oxygen species (ROS) by photochemical processes (Green and Howman 2005). The complex nature of the actual probes (CdSe core, ZnS shell, organic coating, biological conjugate) also means they are large entities (radii can be 5 nm) and therefore may interfere with some aspects of the processes which they are intended to probe purely because of their size. In addition, orange-red emitting labels are desirable in many applications because these wavelengths are not strongly absorbed by cells and the fluorescence from cells themselves is at shorter wavelengths. Longer wavelengths of luminescence correspond to larger particles. Silicon nanoparticles promise to solve some of these problems: (i) there are no heavy metal ions to leach, though it is likely that all semiconductor nanoparticles will generate some reactive oxygen species (ROS) under illumination; (ii) the robust surface chemistry at Si particle surfaces (Lie et al 2002a; Li et al 2004a; Tilley et al 2005) could simplify greatly the probe used (eg, we have shown that DNA can be synthesized directly on nanocrystalline porous Si as a precursor to nanoparticle formation (Lie et al 2004); and (iii) Si nanoparticles as small as ca 2 nm diameter luminesce orange-red (Reboredo and Galli 2005).

It should be noted, however, that Si nanoparticles are much less well understood in terms of their fundamental photophysics than the particles made from direct gap semiconductors such as CdSe (Brus 1994). The photophysics of Si particles is itself an area of much current research interest. This is partly due to the fact that quantum dots of

CdSe and other binary semiconductors are prepared easily by arrested precipitation from reactions of the appropriate metal ion with H_2Se or H_2S. In contrast, the chemical routes to Q-Si are not so controllable, yet. For these reasons, there are few applications of Si nanoparticles in biology at present, though several groups are actively developing the technology.

Cytotoxicity

Recently there have been concerns about the toxicity of nanoparticles including those used as labels in biology. The whole area of nanoparticle toxicology is being actively investigated (Donaldson et al 2004) and when using these particles as biological labels, it should be borne in mind that they may not be inert towards the biological system under study. Nevertheless, in cell biology experiments where long-term exposure is not an issue, the nanoparticles have considerable advantages over many molecular dyes. Semiconductor nanoparticles based on heavy metals can leach metal ions whose toxicity is known, though the conditions and rates of release of such species from the nanoparticles are still being investigated. All semiconductor nanoparticles (or bulk semiconductors) can act as photocatalysts: absorption of light creates electrons and holes which may react with oxygen at the particle surface to produce ROS, eg, superoxide, peroxide, and hydroxyl. Clearly, Si nanoparticles solve the former problem, but further work is required to assess the ROS aspects, as well as other possibilities related to the particle size (Donaldson et al 2000, Wilson et al 2002, Dick et al 2003).

As mentioned, both bulk cadmium (Cd) and selenium (Se) are well-known to be toxic, eg Kondoh et al (2002) reported that cadmium induces apoptosis, partly via caspase-9 activation in HL-60 cells, whilst Shen and colleagues (1999) observed sodium-selenite induced oxidative stress and apoptosis in human hepatoma HepG2 cells. Much of the published work employing quantum dots (QDs) as labels, notes the absence of obvious toxicity. However, relatively little data is available concerning the cytotoxicity of quantum dots made from cadmium and other heavy metal chalcogenides, therefore studies specifically aimed at probing the toxicity of QDs have appeared recently.

In a study by Derfus and colleagues (2004), the cytotoxicity of semiconductor quantum dots using primary hepatocytes as a liver model was probed. They found that CdSe-core QDs were indeed acutely toxic under certain conditions. Their initial observations led them to conclude that process parameters and environmental conditions could dramatically affect the observed toxicity in a hepatocyte culture model.

Their findings indicated that under standard conditions of synthesis and water-solubilization with mercaptoacetic acid (MAA), the CdSe QDs were not cytotoxic. However, if TOPO-coated QDs were initially subjected to air for 30 min and then modified with MAA, a dramatic dose-dependent decrease in cellular viability was observed (from 98% to 21% at a QD concentration of 62.5 μg/ml).

Based on these results, they suspected that oxygen in the air was oxidizing the surface of the CdSe QDs, releasing free Cd^{2+} ions, leading to the observed cytotoxic effects. After exposure to an oxidative environment, a progressive change in the color and absorbance profile of the QD solution was observed, a blue-shift in the excitonic fluorescence spectra, a broad red-shifted fluorescence peak adjacent to the excitonic fluorescence peak, and a decrease in the quantum yield. Shifts in the absorbance and fluorescence spectra occurred because of a decrease in the size of the nanoparticle (loss of surface atoms due to oxidation), while the broad red-shifted fluorescence peak could be attributed to the formation of lower-energy mid gap states induced by newly formed defects. To test their hypothesis, they exposed solutions of MAA-coated CdSe QDs to a UV-light source ($\lambda_{em} = 365$ nm) with a power density of 15 mW/cm^2 for 1–8 h and then incubated with hepatocytes. They observed a 6%, 42%, 83%, and 97% decrease in viability when cells were incubated with CdSe QDs (62.5 μg/mL) after being exposed to UV light for 1, 2, 4, and 8 h. They proposed that the free, ionized cadmium rendered the QD solution cytotoxic via known mechanisms of cadmium hepatotoxicity, ie, binding of thiol groups in the mitochondria (Rikans and Yamano 2000). When the surface was not oxidized, however, they found the Cd atoms on the surface of the nanoparticles remained bound to neighboring Se atoms and to the stabilizing ligand and were relatively innocuous.

Shiohara et al (2004) investigated the cytotoxicity caused by quantum dots by performing cell viability assays to determine the difference in cell damage depending on the sizes and colors of mercapto-undecanoic acid (MUA)-modified quantum dots and cell type. In their study they used three cell types: Vero cell, HeLa cell and primary human hepatocyte, and three MUA-QD types (QD520, QD570, and QD640). These QD-types emitted green, yellow, and red light respectively. Their results showed that cell viability decreased with increasing concentration of MUA-QDs. However, in the case of Vero cell (African monkey's kidney cell) with red fluorescence QD (QD640), the cell damage was less than for the others. Furthermore, through flow cytometry assays, they found that the cell damage caused by MUA-QD turned

out to be cell death after 4–6 h incubation. They suggest that in order to utilize quantum dots in humans, further study should be done on the relationship between the cell type and MUA-QD cell damage. They also suggest an estimate of the mutation rate in bacteria and carcinogenesis in animals should be obtained, and further research into the mechanism of toxicity is also needed. In terms of the quantum dots, they suggest surface processing be re-examined or, new, heavy metal-free materials used to coat the surface of the quantum dots. In particular, they suggest using "new safer QDs, such as silicon-QDs" (Shiohara et al 2004, p 671).

Kirchner and colleagues (2005) extended the studies undertaken by Derfus et al (2004) and Hoshino et al (2004) by investigating the effect of different organic coatings on cytotoxicity. The samples under examination were CdSe, CdSe/ZnS and gold (Au) nanocrystals coated with mercaptopropionic acid (MPA), embedded in either a silica shell or in an amphiphilic polymer shell. Kirchner and colleagues also determined quantitative values for the onset of cytotoxic effects. They observed poisoning of normal rat kidney (NRK) cells due to release of Cd^{2+} ions started at concentrations of $0.65\pm0.12\,\mu M$ and $5.9\pm1.3\,\mu M$ of surface Cd atoms for MPA-coated CdSe and CdSe/ZnS particles respectively. In agreement with the work of Derfus et al (2004) their data showed that the ZnS capping layer increased the critical concentration up to which no toxic effects can by observed by almost a factor of 10. They also found that embedding the particles in a stable ligand shell such as cross-linked silica groups, dramatically reduces the release of Cd^{2+} ions. In the case of PEG-silica coated CdSe and CdSe/ZnS particles no toxic effects were observed up to concentrations of $30\,\mu M$ Cd surface atoms. For polymer-coated particles an additional pathway of poisoning was observed. For polymer-coated CdSe and CdSe/ZnS nanocrystals, cytotoxic effects started at concentrations of approximately $0.80\pm0.04\,\mu M$ and $0.98\pm0.07\,\mu M$ Cd surface atoms respectively. They concluded that in addition to the release of Cd^{2+} ions from the surface of CdSe and CdSe/ZnS nanoparticles, cells could also be impaired if nanoparticles precipitate on the cell surface. Furthermore, cytotoxic effects were different when the particles were ingested by the cells compared to when the particles were just present in the medium surrounding the cells. From this point of view, they suggest that it is important to correlate any study on the cytotoxicity of particles with detailed microscopy analysis regarding the pathway of particle uptake.

Green and Howman (2005) investigated the interaction of water-soluble semiconductor quantum dots with supercoiled DNA. They reported that commercially available water-soluble quantum dots (CdSe capped with a shell of ZnS, complete with biotin functionality) could nick DNA. They attributed this observation to free radicals, both photogenerated and surface oxide generated.

Photodynamic therapy

The work of Derfus and colleagues (2004) provoked the hypothesis from Bakalova et al (2004) that while the cytotoxicity of quantum dots mediated by UV irradiation is harmful for normal cell viability, it may be useful in killing cancer cells. As discussed by Bakalova and colleagues, quantum dots are considered to be energy donors, and the possibility for energy transfer between quantum dot particles and cell molecules (such as triplet oxygen, reducing equivalents, pigments) has the potential to induce generation of reactive oxygen species and/or free radicals and to provoke apoptosis of the cells. They speculated that the dual nature of UV-mediated cytotoxicity of quantum dots and their energy donor capacity could possibly open a new area of quantum dot application in biology and medicine, as novel photosensitizers or at least as potentiators of the conventional photosensitizing drugs in photodynamic therapy of cancer.

The potential of quantum dot bioconjugates to sensitize cells to UV irradiation and to promote the photodynamic activity of the classical photosensitizers such as trifluoperazine (TFPZ) and sulfonated aluminum phthalocyanine (SALPC) was examined (Bakalova et al 2004). Water-soluble CdSe nanocrystals were conjugated with anti-CD antibody with known specificity to leukemia cells. They incubated quantum dot anti-CD conjugates with the leukemia cell line Jurkat to ensure specific interaction with the cell surface. This interaction was confirmed by confocal fluorescence microscopy. Furthermore, they mixed quantum dot anti-CD90 labeled leukemia cells with normal lymphocytes and subjected this mixture to UV irradiation in the presence or absence of a classical photosensitizer (TFPZ or SALPC). The cell fractions were separated by lectin-affinity column chromatography. The cell type was confirmed with fluorescent confocal microscopy and flow cytometry using appropriate antibodies; quantum dot anti-CD90 for leukemia cells and PE-CD44 for normal lymphocytes. They determined the viability of the separated cell fractions using flow cytometry and the methyl tetrazolium test. Their results demonstrated that quantum dot anti-CD conjugates sensitized leukemia cells to UV irradiation and promoted the effect of the classical photosensitizer SALPC.

This result suggests that, under the conditions of their experiment, the UV-induced cytotoxicity of quantum dot anti-CD90 is predominantly a result of local generation of free radicals and reactive oxygen species, which may sensitize Jurkat cells to UV light and/or modify the effect of the classical photosensitizer TFPZ or SALPC. One may speculate also that quantum dots promote the photodynamic effect of TFPZ and SALPC through direct or indirect activation of the photosensitizers and by decreasing photobleaching. However, as discussed by Bakalova and co-workers, if quantum dot anti-CD90 conjugate is to qualify as a real photosensitizer, it has to satisfy several generic requirements for photosensitizers: (i) constant composition; (ii) straightforward synthesis; (iii) no toxicity in the absence of light; (iv) target specificity and good pharmacokinetics; (v) high triplet state yield; (vi) minimal self-aggregation in the body (as aggregation decreases its high triplet state yield); and (vii) avoid degradation processes, eg, photobleaching (Bakalova et al 2004).

Obviously, quantum dot anti-CD conjugates satisfy the first five characteristics. They are compounds with constant composition and synthesis is relatively simple and inexpensive. Bakalova and co-worker's study showed that, at the doses tested, they were not cytotoxic in the absence of light, but have a potential to induce relatively strong cytotoxic effects under UV irradiation. The synthesis of different immunocompatible quantum dot bioconjugates can guarantee their specific localization in the target tissue. More recently, Samia et al (2003) reported that the quantum yield of CdSe-generated singlet oxygen in toluene is approximately 5%. In comparison, the singlet oxygen efficiency of phthalocyanine-based photosensitizers has been calculated to be approximately 43%. However, it is necessary to bear in mind that photobleaching of the classical photosensitizers is more rapid than that of CdSe quantum dots. Prolonged and repetitive exposure of quantum dot treated cells to UV-vis irradiation has the potential to ensure a relatively high steady-state level of singlet oxygen during irradiation, sufficient to induce apoptotic and/or necrotic cell death. As stated initially, all these facts support the hypothesis that quantum dot bioconjugates have the potential to be photosensitizers. However, to qualify them as real photosensitizers it is necessary to verify the last two characteristics mentioned above, as well as to examine the possibility of energy transfer between quantum dots and classical photosensitizers (Bakalova et al 2004).

Silicon nanoparticles
Preparation

Silicon nanoparticles can be made by a variety of routes, which may be classified roughly as "chemical" or "physical". Physical routes generally involve high-temperature and/or vacuum deposition techniques and are favored when the object is to produce small quantities of material for physical or electronic applications and we have therefore restricted our discussion of these methods. Chemical routes tend to produce material of less well-defined composition and size (with some exceptions), but often produce rather large amounts of material and may be compatible with the conjugation of biological molecules at the particle surface. We have therefore emphasized these routes in this survey.

A common starting point for some hybrid preparations is porous Si, typically a film a few microns-thick, produced by electrochemical etching of Si wafer in fluoride media. It is generally considered to luminesce owing to the presence of quantum-confined structures and is often described as a nanocrystalline film. Porous Si can be broken up into individual nanoparticles by a variety of means including ultrasound (Heinrich et al 1992). It therefore provides one of the simplest routes to Si nanoparticles, requiring only a small (3 A, 30 V) power supply (for the etching) and an ultrasonic horn. As there is a large literature on porous Si and reviews of its surface chemistry (Buriak 2002), we discuss mainly preparations of samples consisting of individual Si nanoparticles.

Electrochemical etching and sonication

In 1990, Leigh Canham (1990) was the first person to show that certain porous Si materials can have large photoluminescence (PL) efficiency at room temperature in the visible region. He presented indirect evidence that free-standing Si quantum wires could be fabricated without the use of epitaxial deposition or lithography. His approach used electrochemical and chemical dissolution steps to define networks of isolated wires out of bulk wafers. Mesoporous Si layers of high porosity exhibited visible (red) PL at room temperature, observable with the naked eye under <1 mW unfocused green or blue laser line excitation. This he attributed to dramatic two-dimensional quantum size effects which could produce emission far above the bandgap of bulk crystalline Si. Individual Si nanoparticles with broad size distribution, but bright orange emission were produced from porous Si by sonication a couple of years later (Heinrich et al 1992).

Wolkin et al (1999) prepared porous Si quantum dot samples by electrochemical etching followed by photo-

assisted stain etching of 6 Ω cm *p*-type Si wafers at current densities of 8–50 mA cm^{-2} using 10%–25% HF: ethanol solutions. The stain etching was accomplished under illumination, with a 500 W halogen lamp, and was used to further increase the porosity. Wolkin et al found that depending on the size, the PL of Si quantum dots present in porous Si could be tuned from the near infrared to the ultraviolet when the surface was passivated with Si-hydrogen (Si-H) bonds. After exposure to oxygen, the PL shifted to the red by as much as 1 eV. This shift and the changes in PL intensity and decay time showed that both quantum confinement and surface passivation determined the electronic states of Si quantum dots. They found a theoretical model, in which new electronic states appear in the bandgap of the smaller quantum dots when a Si=O bond is formed, was in good agreement with experimental results.

Sweryda-Krawiec et al (1999) produced colloidal solutions of Si nanocrystals by sonicating porous Si wafers (suspended in 5 mL of degassed toluene) for 60–90 min in closed vials. During sonication, crystallites leached out from the porous Si network and the toluene suspension became pale yellow. Sweryda-Krawiec and co-workers then modified the surface of the Si nanocrystallites using alcohols. Room-temperature addition of 1-undecanol, 1-hexadecanol, 1-octanol, and 1,12-dodecanediol completely quenched the PL of Si nanocrystallites. Heating the nanocrystallites with 1-undecanol, 1-hexadecanol, and 1-octanol resulted in the partial recovery of the PL and in the formation of 1- to 10-nm diameter alcohol-capped Si nanocrystallites. Heating the Si nanocrystallites with 1,12-dodecanediol also partially restored the PL. TEM and AFM images indicated the formation of diol interconnected 100- to 800-nm diameter Si nanoparticle agglomerates.

Belomoin and co-workers (2002) demonstrated that electrochemically etched, hydrogen-capped Si$_n$H$_x$ clusters with *n* larger than 20 are obtained as a family of discrete sizes. These sizes are 1.0 (Si$_{29}$), 1.67 (Si$_{123}$), 2.15, 2.9, and 3.7 nm in diameter. They characterized the particles via direct electron imaging, excitation and emission optical spectroscopy, and colloidal crystallization. The bandgaps and emission bands were measured. The smallest four were ultrabright blue, green, yellow, and red luminescent particles. The blue particles were obtained by brief treatment of the wafer in an ultrasonic bath, where the film crumbled into a colloidal suspension of ultrasmall blue particles. As noted by the authors the availability of discrete sizes and distinct emission in the red, green, and blue (RGB) range is useful for biomedical tagging, RGB displays, and flash memories.

Lie et al (2002a) produced Si quantum dots by refluxing porous Si in toluene solutions of alkenes. The porous layer breaks up under the conditions of the reflux and the alkene is hydrosilated at the particle surface to form a hydrocarbon monolayer which protects the particles and solubilizes them in organic solvents. The size of the Si core of these particles was about 2.5 nm diameter from a combination of PL, STM, and Raman measurements and they can be redispersed in organic solvents and cast as a film (Lie et al 2004; Chao et al 2005).

Cichos and co-workers (2004) and more recently Valenta et al (2005) also prepared colloidal suspensions of Si nanocrystals (NCs) from light-emitting porous Si grains. Valenta et al obtained nanoparticles by mechanical pulverization of electrochemically etched layers. Sedimented and/or filtered Si NCs sols revealed a green PL band around 530 nm, which was interpreted as radiative recombination of electron–hole pairs inside Si NCs with diameter about 2 nm. Single-molecule spectroscopy techniques could be applied to investigate PL of single grains of Si NCs dispersed on substrates from highly diluted solutions. On the other hand, their preparation of concentrated suspensions enabled Valenta et al to fabricate bulk samples with embedded Si NCs or to prepare self-organized nanostructures on surfaces. They acknowledge however there are many technological aspects to improve. In particular, an efficient method to break the micrometer-sized grains of porous Si into sub-micron parts has to be found.

Lee et al (2004) produced white-light-emitting Si nanoparticles, whose surfaces were passivated with butyl, using focused ultrasound. The white light emission was achieved by controlling the size distribution (without the need to add any fluorescent ions). The white-light-emitting Si nanoparticles had a wide size distribution of 1–5 nm with an average size of 2.7 nm, which were sufficiently small to indicate the quantum confinement effect for Si. The PL spectrum covered a wide range (320–700 nm) with a full width at half maximum of approximately 190 nm.

Reactive sputtering

Furukawa and Miyasato (1988) succeeded in fabricating mostly crystalline Si-H materials, which had a wide optical bandgap of up to 2.4 eV by means of a reactive sputtering technique with a low substrate temperature of ~100 K. The structural analysis showed that the materials consisted of small crystalline Si particles surrounded by hydrogen atoms, whose diameters were 20–30 Å. They explained the widening of the optical bandgap by a three dimensional quantum-size effect in the particles.

Sol-gel techniques

Zhang et al (1998) successfully incorporated Si nano-crystallites, extracted from porous Si, into a silica sol-gel matrix. The fundamental properties of the Si nanoparticles, as a consequence of the porous silica matrix and additional passivating agents were examined, with the goal being to diversify the potential applications, by encapsulation in a transparent, robust matrix. Fluorescence microscopy revealed that the light-emitting Si crystallites aggregated into micron-sized domains somewhat unevenly throughout the silica matrix, although this distribution could be improved by employing a surfactant, dioctyl sodium sulfosuccinate (DSS). They also found that the Si nanocrystallites showed stable, intense PL, which was retained over time if a fatty acid was added as a passivating agent.

SiO$_2$ implantation

Kovalev et al (1998) prepared heavily oxidized Si nanocrystals by Si ion implantation in a silicon dioxide (SiO$_2$) layer, with subsequent annealing at $T = 1100$ ºC for 15 minutes.

Self-assembly

Choi et al (1998) fabricated a quantum-dot transistor based on Si self-assembled quantum dots. The dot size calculated from the data was ~7 nm, which was consistent with the size of the self-assembled dots incorporated in the transistor.

Kohno and Takeda (1998) fabricated a self-organized chain of crystalline-Si nanospheres via an extension of the vapor–liquid–solid mechanism. Transmission electron microscopy (TEM), electron energy-loss spectroscopy (EELS), and electron-induced x-ray fluorescence (EIXF) analyses proved that the crystalline Si nanospheres (of about 10 nm in diameter and at a nearly equal spacing), were supported in amorphous silica and carbon. They attributed the self-organization phenomenon to the periodic instability of catalysts and spontaneous oxidization during the growth of nanowhiskers.

Synthesis in inverse micelles

Highly crystalline, size-selected Si nanocrystals in the size range 2–10 nm were grown in inverse micelles by Wilcoxon and colleagues (1999) and their optical absorption and PL properties were studied. High resolution TEM and electron diffraction results showed that these nanocrystals retained their cubic diamond structures down to sizes ~4 nm in diameter, and optical absorption data suggested that this structure and bulk-like properties were retained down to the smallest sizes produced (~1.8 nm diameter containing about 150 Si atoms). High-pressure liquid chromatography (HPLC) techniques with on-line optical and electrical diagnostics were developed to purify and separate the clusters into pure, monodisperse populations. The optical absorption revealed features associated with both the indirect and direct bandgap transitions, and these transitions exhibited different quantum confinement effects. The indirect bandgap shifted from 1.1 eV in the bulk to ~2.1 eV for nanocrystals (~2 nm in diameter) and the direct transition blue-shifted by 0.4 eV from its 3.4 eV bulk value over the same size range. Tailorable, visible, room temperature PL in the range 700–350 nm (1.8–3.5 eV) was observed from these nanocrystals. The most intense PL was in the violet region of the spectrum (~365 nm) and was attributed to direct electron-hole recombination. Other less intense PL peaks were attributed to surface state and to indirect bandgap recombination.

Tilley et al (2005) formed Si nanocrystals in inverse micelles by the solution reduction of Si tetrachloride with strong hydride reducing agents at room temperature and pressure. The Si nanocrystals were then capped with 1-heptene, purified and redispersed into hexane and showed strong PL in the visible regime. Colloidal suspensions of the 1-heptene Si nanocrystals were stable and photoluminescent for at least 6 months in air, showing their resistance to photo-oxidation.

Laser ablation

Hata and co-workers (2001) demonstrated the use of a self-assembled monolayer (SAM) of hexanethiol on epitaxial Au(111) surfaces as a template to deposit in-situ Si nanoparticles fabricated by laser ablation. Scanning tunneling microscopy (STM) and atomic force microscopy (AFM) observations, in addition to PL measurements showed that the Si nanoparticles deposited in situ on SAMs were round shaped, firmly attached to the surface, and remained stable for at least a couple of months. They found control over the size of the Si nanoparticles, in the region where the quantum confinement effect is important, could be easily achieved by changing the argon (Ar) ambient pressure. As noted by the authors, this result suggests the possibility of fabricating thin layers of Si nanoparticles that have controlled optical and electronic properties. In situ deposition is important since subsequent processes such as vacuum deposition could be carried out sequentially to fabricate electronic contacts or protecting capped layers without exposing these easily oxidized materials to air.

Thermal annealing

In 1996, Schoenfeld and co-workers (1996) formed Si quantum dots (in nanocrystalline Si) by crystallizing amorphous Si thin films, deposited on Si(110) substrates, using a rapid thermal annealing technique. Room temperature PL (using the 338 nm line of an N_2 laser for excitation) showed intense blue light emission from the Si quantum dots in the nanocrystalline thin films. The luminescence band between 2.6 and 3.2 eV consisted of distinct peaks.

Liu and colleagues (2005) successfully synthesized luminescent Si nanoparticles which were redispersible in various solvents. The nanoparticles were prepared through annealing and subsequent etching with HF from amorphous SiO_x (x<2) powders as starting materials. Due to a slow etching process, a narrow size distribution (~12% in polydispersity) was achieved for a typical sample. Photoluminescence, from the ultraviolet to the visible region, under excitation at the energy corresponding to direct bandgap transition was observed from the HF-etched samples. Liu et al's TEM observations showed the different disperse morphology of Si particles when dispersed in different solvents. At low concentrations, the nanoparticles distributed randomly with inhomogeneous distance in methanol, scattered in an isolated fashion with very large distance in octanol, and arranged themselves densely in toluene. When suspended in octanol at high concentrations, they observed the Si particles tended to self-assemble into large aggregates (~66 nm).

Kapaklis et al (2005) produced photoluminescent Si nanocrystals by the simple disproportionation reaction of SiO. For annealing temperatures of 900–950°C, the nanocrystals produced exhibited a broad size distribution with a distinct maximum in the range of 4–4.5 nm. The nanocrystals were spherical in shape and isolated inside an amorphous oxide matrix, as revealed by high-resolution transmission electron microscopy (HRTEM) analysis. All samples exhibited strong PL even at room temperature with three emission bands at 1.33, 1.52, and 1.67 eV. The authors state the first band originates from excitonic recombination in the Si nanocrystals. They attributed the bands at higher energy to the presence of α-Si clusters in the samples and the gradual transition of these clusters to the crystalline state, since the annealing temperatures were not enough to fully disproportionate and crystallize SiO and, for a given cluster size, the bandgap in α-Si is smaller than in crystalline Si. The authors also suggest that the disproportionation of bulk SiO could be a suitable method for the production of Si-based light emitting materials in large quantities.

Thermal vaporization

Dinh et al (1996) synthesized thin films of Si nanoclusters passivated with oxygen or hydrogen, with an average size of a few nanometers, by thermal vaporization of Si in an argon (Ar) buffer gas, followed by subsequent exposure to atomic hydrogen. HRTEM and x-ray diffraction (XRD) analyses revealed that these nanoclusters were crystalline. All samples showed strong infrared and/or visible PL with varying decay times from nanoseconds to microseconds, depending on synthesis conditions. Absorption in the Si cores for surface passivated Si nanocrystals was observed by PL excitation spectroscopy. They noted the visible components of the PL spectra blueshifted and broadened as the size of the Si nanocrystals was reduced.

van Buuren and co-workers (1998) also prepared Si nanocrystals using the same thermal vaporization technique as Dinh et al (1996) and went on to study the changes in the electronic properties of the nanocrystallites as a function of particle size. They observed shifts in both the conduction band and valence band edges, indicating quantum size effects in the band structure of the nanocrytals, and for the first time were able to correlate these shifts with a known size of nanocrystal. They found the general trend of the bandgap versus size curve agreed well with theory, but in all cases the experimental bandgap was smaller than the theoretical prediction.

Decomposition of silanes

Littau and colleagues (1993) described a high-temperature aerosol apparatus for the synthesis of 3–8 nm, surface-oxidized Si crystallites. The particles were made by homogeneous gas-phase nucleation following pyrolysis of dilute disilane in helium. The particles were collected as a robust ethylene glycol colloid, and characterized by TEM, X-ray powder Bragg scattering, HPLC, infra-red, and optical spectroscopy. The particles exhibited a shell structure, with a crystalline Si core of bulk lattice constant, capped with ~1.2 nm shell of SiO_2. After acidic reflux, the particles luminesced with 5% net quantum yield. As the Si core decreased to about 2 nm, the emission shifted 0.5 eV above the bulk Si bandgap. This red luminescence was consistent with the predicted quantum size effect in crystalline Si.

Fojtik and Henglein (1994) prepared crystalline Si particles, which were coated by an oxide layer, by combustion of silane. Red or orange luminescence was activated by etching these particles in a 1:1 cyclohexane/propan-2-ol suspension by aqueous hydrogen fluoride in the presence of air. They observed that when a suspension of luminescent particles in cyclohexane was mixed with polar solvents such as alcohol,

ether, and chloroform, the luminescence was more or less quenched (depending on the nature of the added solvent). Mixing with non-polar solvent such as carbon tetrachloride did not lead to quenching. Triethylamine and ammonia were found to quench the luminescence extremely effectively, as did sulfuric acid. They also observed that the particles migrated in an electric field in different directions depending on the chemical surface treatment. Fojtik and Henglein concluded that luminescence occurs when the particles carry only a few oxidized centers on the surface, and that the protonation state of these centers strongly affects the luminescence.

A synthetic method was developed by Holmes et al (2001) to produce robust, highly crystalline, organic-monolayer passivated Si nanocrystals in a supercritical fluid. By thermally degrading a Si precursor, diphenylsilane, in the presence of octanol at 500°C and 345 bar, they reported that relatively size-monodisperse, sterically stabilized Si nanocrystals, ranging from 15 to 40 Å in diameter, could be obtained in significant quantities. The absorbance and PL excitation spectra of the passivated nanocrystals exhibited a significant blue shift from the bulk bandgap energy of 1.2 eV due to quantum confinement effects. The Si clusters also showed efficient blue (15 Å) or green (25–40 Å) band-edge photoemission with luminescence quantum yields up to 23 % at room temperature. This study also reported that the smallest size-monodisperse 15 Å diameter Si nanocrystals exhibited previously unobserved discrete electronic absorption and luminescence transitions (due to quantum confinement effects).

English et al (2002) produced sterically stabilized Si nanocrystals by arrested precipitation in solvents, heated and pressurized above their critical points to temperatures ranging from 400 to 500°C. These temperatures were sufficient to degrade the organosilane precursors (such as diphenylsilane) to Si; to promote Si crystallization in the nanocrystal core; and to initiate surface binding of organic capping ligands. English and co-workers showed that organic monolayer coated Si nanocrystals, ranging from 1 to 10 nm in diameter, emitted with nanosecond-scale lifetimes and high quantum yields, making it possible to measure the PL spectra of single Si quantum dots. The Si quantum dots demonstrated stochastic single-step "blinking" behavior and size-dependent PL spectra with line widths approximately only three times greater than those measured for CdSe nanocrystals at room temperature.

Silicon nanoparticles with an average diameter of 5 nm were prepared by Li et al (2003) using CO_2 laser-driven pyrolysis of silane. After HF/HNO_3 etching, Si nanoparticles

with controlled visible luminescence were produced. They controlled the wavelength of maximum PL emission from the nanoparticles, from above 800 nm to below 500 nm, by controlling the etching time and conditions. Characterization of the particles by XRD, X-ray photoelectron spectroscopy (XPS), and Fourier Transform Infra-Red (FTIR) spectroscopy confirmed that crystalline Si structures were present in both the original and etched particles. The expected XRD peak broadening with decreasing particle size was observed. Rapid thermal oxidation of orange emitting particles produced blue-emitting particles with peak PL emission near 420 nm. They also found the PL from particles after etching could be stabilized significantly by chemical oxidation using HNO_3.

Solution synthesis

Bley and Kauzlarich (1996) developed a solution synthesis, reacting the Zintl compound KSi, with $SiCl_4$ (at significantly lower temperatures than previously required), to produce crystalline Si nanoparticles. In addition, the reaction was performed at ambient pressure and yielded a particle surface that could be modified by chemical methods. The same group (Mayeri et al 2001) later carried out a nuclear magnetic resonance (NMR) study of the synthesis of alkyl-terminated Si nanoparticles from the reaction of $SiCl_4$ with the Zintl salt, NaSi. The samples studied were found to be a mixture of nanocrystalline and amorphous Si nanoclusters. Interpretation of the primary peaks in the NMR was consistent with alkyl termination of the Si nanoclusters.

In a later paper (Baldwin et al 2002) this group concluded that there were problems with the synthetic methodology involving Zintl compounds. The yields were generally low, the reaction was difficult to scale up, and the heterogeneous nature of the reaction mixture led to little potential for control over the size, as the initiation of the reaction and thus nucleation occurred over an extended time. They went on to report the reaction of Si tetrachloride with sodium naphthalide in 1,2-dimethoxyethane to give a halide capped Si nanoparticle (mean diameter 5.2±1.9 nm) that could then be terminated with n-octanol. The sample exhibited PL in the 410–430 nm range with an excitation at 320 nm; however they acknowledged better size control would be necessary to probe the optical properties.

Also in 2002, Liu and Kauzlarich (2002) described a new synthetic route for the synthesis of hydrogen terminated Si nanoparticles. The nanoparticles were prepared by the initial reaction of the metal silicide, Mg_2Si, with either $SiCl_4$ or Br_2 and subsequently with $LiAlH_4$. These reactions produced Si nanoparticles with surfaces that were covalently

terminated with hydrogen. The resultant nanoparticles could be suspended in organic solvent and were characterized by FTIR, UV-vis absorption, and PL spectroscopy.

Zou et al (2004) synthesized Si nanoparticles (~4.5 nm in diameter) from a room-temperature solution route, terminated by a silanization method for the first time. Energy-selected emission was observed, consistent with the distribution of sizes obtained by this route. The silanized Si nanoparticles were compared with Cl-terminated Si nanoparticles and octoxy-terminated Si nanoparticles. All three differently terminated NPs luminesced in the same region. However, being susceptible to hydrolysis and subsequent decomposition, the Cl-terminated Si nanoparticles were found to degrade and lose their PL over time. The octoxy-terminated Si nanoparticles, although more stable than the Cl-terminated nanoparticles, also degraded over a slightly longer time. The PL intensity of the silanized Si nanoparticles sample remained approximately constant for two months, and showed photochemical stability for up to one year.

Hybrid techniques

Botti et al (2001) synthesized light-emitting layers of Si quantum dots embedded in a diamond matrix using a hybrid chemical vapor deposition-powder flowing technique. Their investigation into the structural and optical properties of the composite films revealed that the insertion in the matrix did not effect the energy range of the emission band. They also found that the emission properties of the Si nanoparticles were stable on storing the samples in ambient atmosphere for a period of one year.

Plasma processing

In 2005, Mangolini et al (2005) presented a single-step continuous flow non-thermal plasma process that produced luminescent Si nanocrystals between 2 and 8 nm on time scales of a few milliseconds. Process yields of 14–52 mg/h of luminescent particles were demonstrated, and they suggest the process is easily scalable through parallelizing.

Giesen et al (2005) investigated the formation and growth of Si nanoparticles from silane in a microwave reactor. The silane was added to the plasma gases Ar/H_2, resulting in the formation of the Si nanoparticles. They then performed experiments to investigate the influence of the process parameters on the size of the produced particles. A molecular beam technique was used together with a particle mass spectrometer (PMS) for sizing the product particles. They also collected and analyzed particles by TEM, surface adsorption (BET), and XRD. The particles were found to lie in the 5–8 nm range and consisted of crystalline Si. They also carried out simulations of the described experiments on an ultra simple thermal plasma model. They found the absolute size of the primary particles was in good agreement with experimental results.

Blue luminescent Si nanoparticles were synthesized from a mixture of argon/silane in a continuous flow atmospheric-pressure microdischarge reactor by Sankaran and colleagues (2005). Particles nucleated and grew to a few nanometers (1–3 nm) in diameter before their growth was abruptly terminated in the short residence time microreactor. Narrow size distributions were obtained. The "as-grown" Si nanoparticles collected in solution were found to exhibit room-temperature PL that peaked at 420 nm with a quantum efficiency of 30%; the emission was found to be stable for months in ambient air.

Physical properties of Si quantum dots

Morphology, PL, and electronic structure in oxidized Si nanoclusters were studied by Carlisle and colleagues (2001). They established the dependence of quantum size effects on bonding structure in oxidized Si nanoclusters by correlating PL data with photon-yield electronic structure measurements. The nanoclusters were synthesized using a laser ablation technique that utilizes a convective helium (He) environment to control the size of the particles. Their conclusion was that the as-synthesized nanoclusters consisted of a pure, crystalline Si core within a nearly pure SiO_2 shell, with little or no sub-oxides present. As the nanoclusters oxidized, the radius of the crystalline core decreased in size, which gave rise to the change in the position of the PL signal.

Belomoin and co-workers (2004) examined the changes in the x-ray structure factors of Si nanocrystals, as a function of size over the 1–6 nm range. They examined how the scattering evolved from broad features to sharp peaks as the particle size increased. The transition from amorphous/molecular-like to polycrystalline-like behavior was found to occur at 2.15 nm. They also found that very little change takes place for clusters of diameters larger than 5 nm.

In 2004, Cichos and co-workers (2004) studied the emission intermittency in Si nanocrystals. They found that the photophysics of Si nanocrystals is of similar complexity as for II-VI semiconductor nanocrystals. Silicon nanocrystals showed an emission intermittency, which was governed by power law statistics for the on and the off times. The off time statistics was intensity dependent and revealed several photoinduced ionization processes, which were interpreted in terms of Auger-assisted and non-Auger-assisted tunneling

processes. Furthermore, they demonstrated that blinking, bleaching, and emission recovery of Si nanocrystals were directly related to each other.

Sychugov and colleagues (2005) used single-dot luminescence spectroscopy to study the emission linewidth of individual Si nanocrystals from low temperatures up to room temperature. The results showed a continuous line narrowing towards lower temperatures, with a linewidth as sharp as 2 meV at 35 K. They asserted that this value proves the atomic-like emission from Si quantum dots subject to quantum confinement.

Reboredo and Galli (2005) examined the theory of alkyl-terminated Si quantum dots by carrying out a series of ab initio calculations to investigate changes in the optical properties of Si quantum dots as a function of surface passivation. In particular, they compared hydrogen-passivated dots with those having alkyl groups at the surface. Alkyl passivation weakly affects optical gaps of Si quantum dots, while it substantially decreases ionization potentials and electron affinities and affects their excited state properties. On the basis of their results, they proposed that alkyl-terminated quantum dots may be size selected, taking advantage of the change in ionization potential as a function of the cluster size. They also point out that some of the reported preparations of Si nanoparticles utilize conditions under which the formation of Si carbide might be expected. This might be the origin of the blue luminesce in some cases where the particle size and the reported luminescence wavelength do not agree with calculations.

This group also carried out an earlier study (Reboredo et al 2004) on the computational engineering of the stability and optical gaps of alkylated Si quantum dots, between 1 and 3 nm. Their calculations showed that surface composition and termination play a dominant role in determining the optical gaps and thermodynamic stability of these nanoparticles. In particular, they found that the optical gap of cubic Si quantum dots could be engineered as a function of their size and surface composition to obtain absorption and emission from the UV to the green.

Photophysical properties of Si nanoparticles
Color of the photoluminescence

In general, Si nanoparticles prepared by gas-phase or by electrochemical methods show orange-red luminescence, whereas those produced by liquid-phase synthesis (Yang et al 1999; Warner et al 2005) often emit blue light despite sometimes being of similar size. These observations and other studies of the PL of porous Si gave rise to some controversy over the assignment of the transition responsible for the luminescence and the details are still not settled. Some clear conclusions have been drawn about various aspects, however, and we briefly review these here because they are relevant for the design of Si-based luminescent probes.

The classic signature of quantum confinement is the observation of size-dependent optical absorption or PL. Silicon, in bulk, has an indirect gap at 1.1 eV which is expected to be size-dependent and a direct gap at 3.4 eV which is not expected to be strongly size-dependent (Brus 1994). The absorbance above the 1.1 eV threshold is weak and unstructured, therefore size-dependent PL measurements have been crucial (Ding et al 2002; Ledoux et al 2002). Using a pulsed CO_2 laser to pyrolyze silane in a gas flow reactor and a molecular-beam chopper synchronized to the laser, Ledoux et al (2002) were able to separate Si nanoparticles by size and demonstrate clearly the blue-shift of the luminescence peak with particle diameter. Over the range of particle diameters from 3 nm to 8 nm, their results match rather well the theoretical curve calculated on the basis of an LCAO treatment, $E = E_{bulk} + 3.73.d^{-1.39}$ (Delerue et al 1993) where d is the particle diameter, E the energy (in eV) of the luminescence peak, and E_{bulk} the bulk bandgap. The smaller particles emitted lower photon energies than expected: this is thought to be due to traces of oxide which was shown in an important paper on porous Si (Wolkin et al 1999) to introduce a level in the gap that limits the maximum observed PL energy to about 2.1 eV.

More sophisticated electronic structure calculations have been made, but for particles > ca 2.5 nm diameter, the PL energy can be understood on the basis of quantum confinement. For smaller particles, the surface termination, especially the role of oxygen, becomes more important because the ratio of surface to bulk Si atoms increases. Two effects should be considered: (i) traces of oxide introduce mid gap states and (ii) a complete O-termination of the surface can drastically alter the properties of the HOMO and LUMO[2]. The first effect is thought to explain why porous Si structures prepared under anerobic conditions emit blue light, but upon exposure to oxygen, emit red (Wolkin et al 1999). The second case has been studied by density functional calculations on Si nanoparticles of diameter 1.1 and 1.4 nm (Zhou et al

---

[2] HOMO = highest occupied molecular orbital and LUMO = lowest unoccupied molecular orbital. The HOMO-LUMO gap in molecules/nanoparticles is analogous to the bandgap of bulk materials.

2003). These authors compared the nature of the HOMO and LUMO for the cases where the surface Si atoms were bonded to H atoms versus –OH groups. A dramatic lowering of the bandgap for the –OH termination, red emission, and a dipole-forbidden transition as in pure bulk Si (indirect gap) was observed, but blue emission from a dipole allowed transition was calculated for the H-terminated particles. It is worth noting that the blue PL from some rather large particles (Yang et al 1999) might be due to a dipole-allowed transition analogous to the direct gap observed in bulk Si at 3.4 eV (Wilcoxon et al 1999; Garoufalis et al 2001). Recent calculations on alkylated Si nanoparticles up to about 2 nm diameter show a reduction of the bandgap compared with H-termination of about 0.2 eV and a larger shift of the orbital energies towards vacuum (Reboredo and Galli 2005). All the computational studies clearly show that in small particles, the surface has to be considered explicitly and it is not sufficient to regard it as simply a boundary condition on the wavefunction of electrons in the core of the particle. As the particle diameter increases, the orbitals are largely determined by the core Si atoms and the simple quantum confinement models work better.

However, the assignment of PL spectra in Si nanoparticles is still not simple because the experimental literature shows examples of blue luminescence from C-implanted porous Si (Liu et al 2001), oxidized porous Si/Si nanoparticles (Bley et al 1996, Germanenko et al 2000) and, in fact, bulk SiO_2 shows blue PL (Itoh et al 1989). A possible role of SiC, which is calculated to increase the bandgap, in nominally Si nanoparticles (Reboredo and Galli 2005) has also been suggested. Further, it is quite common for oxidation of Si nanoparticles to cause a shift in the PL from red to blue (Li et al 2003; Chao et al 2005). Although this might be interpreted as a decrease in the diameter of the Si core, the calculations of Zhou et al (2003) predict red luminescence for O-termination and might be used to infer that the blue PL in these cases originates instead from Si oxides. We and others (Sham et al 2004) have found X-ray and vacuum ultraviolet-excited PL to be of use in the assignment because the initial absorption involves localized electronic states and can be correlated with the photoemission spectra. The blue PL in alkylated Si nanoparticles prepared by an electrochemical method, and subsequently oxidized, was determined to originate from excitation of oxidized Si atoms (Chao et al 2005). Clearly, the observation of blue or red luminescence and a determination of elemental composition is not sufficient to deduce the nature of the transition: a detailed photophysical and spectroscopic study is probably required for each new synthesis.

Photophysical properties relevant to biological imaging

Ideally, luminescent labels for biological imaging should emit in a region of the spectrum where cells do not, should have a fast radiative recombination rate, should be stable, water-soluble, and have a high luminescence quantum yield. A fast radiative recombination rate allows many photons to be emitted from a given particle during the imaging and therefore can be important for the sensitivity. Typically Si nanoparticles which emit red light do so via dipole-forbidden transitions with microsecond or longer lifetimes (Puzder et al 2003) whereas the blue-emitting particles show nanosecond lifetimes typical of dipole-allowed transitions (Wilcoxon et al 1999; Warner et al 2005). Which type of particle is better depends the particular application: clearly red-emitters are more suitable if autofluorescence is the major problem, but in some applications they may suffer from slow radiative recombination. In bulk Si, the bandgap at 1.1 eV is indirect and emission of light is slow because simultaneous emission/absorption of a lattice vibration (phonon) is necessary to conserve crystal momentum and nonradiative processes dominate. Although nanoparticles do not have the full translational symmetry of the bulk solid, the red emission still retains the characteristics expected for an indirect gap and long excited-state lifetimes are often observed, nevertheless, the nonradiative pathways are dramatically slowed and the PL quantum yield can be high even for the red-emitting particles (Brus 1994). However, as noted in the previous section, the surface termination may have a strong influence on the excited state and in some cases (nanoparticles prepared by decomposition of diphenylsilane in supercritical fluids (English et al 2002)) lifetimes ca. 6 ns have been observed for particles emitting at wavelengths as long as 680 nm (red). The authors argue that the radiative rates of ca. $4 \times 10^7 \, s^{-1}$ deduced from the lifetime and the quantum yield reflect dipole allowed transitions even in their largest (d=6.5 nm) particles because of strong coupling between the core and surface states. Finally, some measurements have been performed on individual Si nanoparticles produced by sonication of porous Si: the lifetime (2.2 μs) of individual particles was measured and it was observed that some particles are dark and the luminescence originates from a small fraction whose quantum yield is almost 100% (Credo et al 1999).

Stability towards photobleaching is one of the important advantages of quantum dots over molecular fluorophores, however Si nanoparticles are not immune (English et al 2002). Bare Si nanoparticles may also be sensitive to quenching by various functional groups (Kirkey et al 2005)

as is known in the case of porous Si (Lauerhaas et al 1992). Capping the particles with an alkyl monolayer stabilizes them towards oxidation except under extreme conditions (Lie et al 2004; Chao et al 2005). However, at high photon fluxes, a reversible bleaching occurs that is related to the luminescence intermittency ("blinking") phenomenon (Efros and Rosen 1997). This is thought to be due to charging/discharging of the particles (Credo et al 1999; Cichos et al 2004) and may lead to irreversible oxidation if the Si core is exposed to air or water (Chao et al 2005). Measurements on single Si nanoparticles produced by sonication of porous Si have been also used to study this process which is a topic of current theoretical interest (Tang and Marcus 2005).

Surface functionalization

Jang et al (2003) demonstrated the incorporation of organic-capped Si nanoparticles into the hydrophobic interior of phospholipid vesicle bilayers, and used PL quenching to determine the accessibility of membrane-embedded nanoparticles to aqueous and lipid-bound quenchers. Experiments with water-soluble quenchers indicated the existence of two populations of membrane-bound nanoparticles with varying accessibilities to the aqueous phase. Results from membrane-bound quenchers revealed that the major population localized deep inside the bilayer. The ability of the nanoparticles to fully embed in the bilayer allowed studies of their interactions with both aqueous and lipophilic molecules in a biomimetic environment. The authors speculate these composites may prove useful in the development of aqueous-based sensors and provide a model system for studying nanoparticle/cell interactions.

Work carried out in our own group resulted in a colloidal suspension of luminescent Si particles, when porous Si prepared at high current densities was refluxed in toluene solutions of alkenes under conditions which allowed hydrosilation to occur (Lie et al 2002a) (see Figure 5). The alkyl monolayer on the surface of the Si particles rendered the colloid lyophilic and stable against flocculation over 14 days. Luminescent nanoparticles were prepared using 1-octene, 1-undecene, and difunctional unsaturated molecules such as dimethoxytrityl protected undecenol and 1,9-decadiene. The dry Si powder could be re-suspended in solvents such as toluene, dichloromethane, and trichloromethane and these suspensions were also similarly stable against flocculation. Fluorescence spectra of the luminescent colloid showed a peak wavelength for the emission at 670 nm. Matrix-assisted laser desorption ionization–time of flight (MALDI–TOF) mass spectra of the colloid showed a broad band for m/z
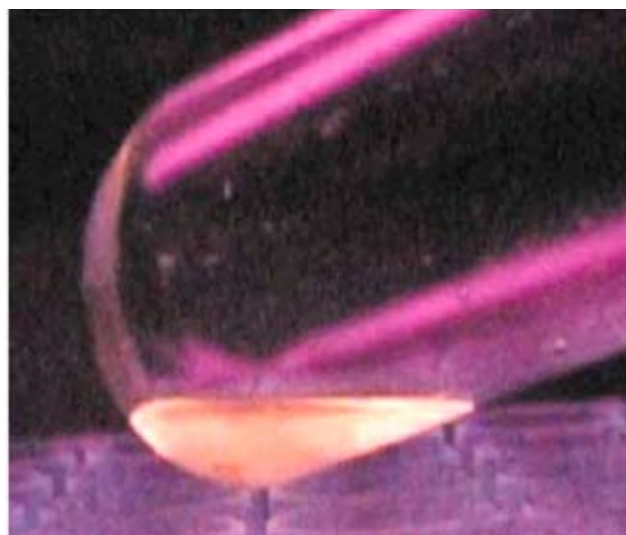
Figure 5 The alkylated Si colloid dispersed in toluene, fluorescing under a UV-lamp (365 nm). The purple glare is due to the effect of reflected light from the walls of the flask on the digital camera used. Reprinted with permission from Lie LH, Duerdin M, Tuite EM, et al. 2002a. Preparation and characterization of luminescent alkylated-silicon quantum dots. *J Electroanal Chem*, 538-9. Copyright © 2002 Elsevier.

between 1500 and 3000 Da. Assuming this feature was due to singly charged ions and the bulk density of Si applied, it set a lower limit on the Si particle radius of about 0.7 nm. This value is consistent with the radius range (1.4–1.7 nm) for the Si core deduced from the emission maximum of the PL spectrum and published particle size-bandgap correlations.

Li et al (2004a) investigated surface functionalization of Si nanoparticles, which they produced using their previously reported technique (ie, laser-driven pyrolysis of silane, followed by HF/HNO$_3$ etching). Alkenes, such as octadecene and undecylenic acid, were attached to the particle surface via hydrosilylation reactions. FTIR spectra confirmed that these reagents were covalently bound to the Si surface. Si-OH terminated surfaces were generated by washing the particles with 20% HNO$_3$ or with concentrated sulfuric acid and hydrogen peroxide. They found commercially available silanes could be attached to this surface, and the FTIR results confirmed that octadecyltrimethoxysilane had been covalently bound to the Si surface. These coated particle dispersions were clear and could easily pass through 0.1 μm filter paper. Surface coating of Si nanoparticles increased the stability of their PL substantially. Dispersions of octadecene-coated particles could be stored in air under fluorescent lighting for months without any measurable change in PL peak position or any decrease in PL intensity. Untreated samples experienced significant changes in PL peak position and intensity over a period of a few days. The surface-treated

particle dispersions could be purified by dialysis and size exclusion chromatography. Li et al found it was crucial to remove excess organic reagents from the particle dispersion in order to obtain high-quality TEM images and to prevent interference with subsequent processing of the particles. TEM imaging confirmed that there were crystalline nanoparticles, with sizes less than 5 nm, in the surface-treated, luminescent particle dispersion. Size-selective precipitation provided an additional means of tuning and narrowing the PL spectra.

Graft polymerization was used for the first time by Li et al (2004b) to prepare a dense conductive polymer coating on free-standing luminescent Si nanoparticles. The nanoparticles were first surface hydroxylated and then reacted with (3-bromopropyl)trichlorosilane to form a dense bromopropylsilane monolayer. This was further reacted with aniline, which displaced the bromine atoms. The surface-bound aniline molecules were then used as active sites for the graft polymerization of polyaniline (PANI). The composition, structure, morphology, and other physical properties of the PANI-capped Si nanoparticles were examined by XPS, FTIR, XRD, and TEM. The silane self-assembled monolayer effectively protected the Si particles against PL quenching and degradation in basic solutions that rapidly quench the PL of unprotected particles. They found the PANI coating further enhanced this protection.

Hua et al (2005) developed an improved etching procedure (using a mixture of HF (48 wt %) and HNO_3 (69 wt %) (10:1 v/v) to generate luminescent Si nanocrystals with very high Si-H coverage and low oxygen content on their surface (see Figure 6). When the desired emission color was reached, they slowed the etching by adding about 10 mL of methanol or a methanol/water mixture (1:3 v/v). This enabled efficient grafting of various molecules containing a terminal double bond onto the particle surface via UV-initiated hydrosilylation reactions. The resulting covalently bound monolayers were able to protect the particles from chemical attack and partially protect them from PL quenching by triethylamine. The organic monolayer also allowed formation of stable

nanoparticle dispersions in a variety of solvents. They also found that chromatographic separation of the particles by size was possible. Monomers including styrene, vinyl acetate, and ethyl undecylenate provided functional groups useful for carrying out further derivatization. Vinyl acetate and ethyl undecylenate grafted Si could be hydrolyzed to generate alcohol and carboxylic acid functional groups. Reaction with 1-hexen-5-ol and undecanol directly provided an alcohol-functionalized surface.

Asanuma et al (2005) studied the kinetic control of the photochemical reactivity of hydrogen-terminated Si with bifunctional molecules. The photo-reactivities of undecylenic acid, undecanoic acid, and 1-dodecene toward hydrogen-terminated Si were investigated by attenuated total reflection fourier transform infrared (ATR-FTIR) spectroscopy, wetting measurements, ellipsometry, AFM, and high resolution electron energy loss spectroscopy (HREELS). Both termini of the bifunctional molecule (eg, undecylenic acid) were found to be reactive, but the alkene was found to react substantially faster than the carboxy group. By optimizing the UV irradiation time, they found it was possible to prepare the high-quality -carboxy functionalized Si surface by minimizing the reaction between the carboxy terminus and the H-Si. More importantly, Asanuma et al observed that the carboxy-terminated monolayers prepared by this one-step process were comparable in terms of surface overage and molecular packing to those obtained via the photochemical reaction of H-Si with ethoxy undecanoate and subsequent hydrolysis.

Bioconjugation of silicon quantum dots

Wang and co-workers (2004) reported a conjugation process that allows labeling of Si nanoparticles with an oligonucleo-tide in aqueous solutions. The Si nanoparticles were produced using lateral electrochemical anodization. They successfully conjugated 1- to 2-nm diameter Si nanoparticles to a 5'-amino-modified oligonucleotide (60mer) that contained a C6 linker between amide and phosphate groups. The conjugation
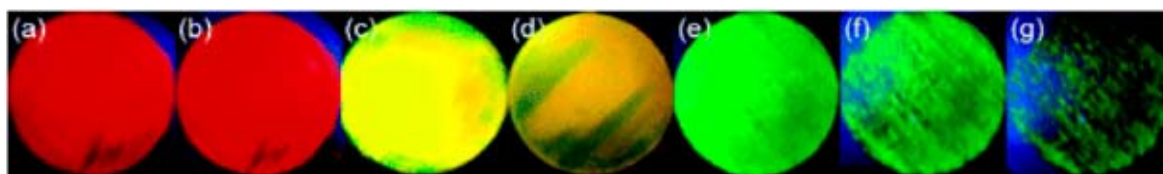
Figure 6 Photo-oxidation of particles under 355 nm UV excitation in air. Red-emitting particles (a) initially and (b) after 10 min illumination. Yellow-emitting particles (c) initially and (d) after 3 min illumination. Green-emitting particles (e) initially, (f) after 20 s illumination, and (g) after 40 s illumination. Reprinted with permission from Hua FJ, Swihart MT, Ruckenstein E. 2005. Efficient surface grafting of luminescent silicon quantum dots by photoinitiated hydrosilylation. *Langmuir*, 21:6054-62. Copyright © 2005 American Chemical Society.

was implemented via two photoinduced reactions followed by a DNA labeling step through formation of a carboxamide bond. Photoluminescence of the conjugates was dominated by two blue bands (400 and 450 nm maximal) under 340 nm excitation. The quantum yield of oligonucleotide-conjugated nanoparticles was determined to be 0.08 as measured against quinine sulfate in 0.1 M $HClO_4$ as a reference standard. However, the authors conclude that ways to reduce size inhomogeneity and surface defects of Si nanoparticles in order to achieve narrower and brighter PL still need to be addressed.

Our group (Lie et al 2004) has successfully conjugated oligonucleotides to nanocrystalline porous Si by direct solid-phase synthesis. Carrying out multi-step synthetic procedures on free nanoparticles is often inconvenient because it may be difficult to separate the excess reagents from the derivatized nanoparticles. However, solid phase synthesis is ideally suited for such processes; therefore, we investigated the possibility of derivatizing the porous Si structure prior to breaking up the layer to form nanoparticles. In this case, the porous Si was produced at a relatively low current density (12.7 mA cm^2 for 6.5 min) which led to the formation of a smooth, black layer (Lie et al 2002b) which was stable, mechanically speaking, to the stresses involved in repeated synthesis/washing steps (Pike et al 2002). Reaction of this layer with dimethoxytrityl-protected 1,10-undecenol (under conditions of reflux) in toluene or mesitylene produced an alkylated porous Si layer, as characterized previously by FTIR (Bateman et al 1998). The alkylated surface now possessed suitable reactive groups to allow automated solid-phase DNA synthesis to be carried out. We found that the synthesis proceeded with an efficiency comparable to that on conventional supports (porous glass, SiO_2), but in order to avoid etching of the Si surface the final, basic deblock procedure was best carried out using the gaseous methylamine protocol (Reddy et al 1997) and Ultramild™ phosphoramidite reagents. Quantitative hybridization studies showed that about 47% of the DNA on the porous Si was accessible and could form duplexes with complementary strands in solution.

Biological applications of Si quantum dots

For Si quantum dots to be used in biomedical applications it is desirable that they have (i) a substantial PL quantum yield in the visible region and (ii) are water soluble and hydrophilic to prevent aggregation and precipitation in a biological environment (Warner et al 2005). Although there are far fewer studies on the biological applications of Si quantum dots in the literature compared with their heavy metal counterparts, some work has been carried out on nanoporous microparticulate Si. This nanoporous microparticulate form of Si has shown great promise in terms of compatibility and cytotoxicity, compared with conventional quantum dots. This work on microparticulate Si is discussed below, in addition to early reports on the biological applications of Si quantum dots.

Chin et al (2001) explored the compatibility of primary hepatocytes with oxidized nanoporous Si. The aim of this study was to characterize the attachment, viability, and function of primary rat hepatocytes, a notoriously difficult cell to grow in culture. Attachment and viability were assessed by fluorescent microscopy of cells probed with vital dyes on nanoporous Si, in contrast to bulk metabolism assays that have been used previously. To investigate the long-term effects of the porous Si material on cell viability and function, they examined the maintenance of liver-specific functions over two weeks of continuous culture. The attachment and spreading of primary hepatocytes on nanoporous Si were compared across a variety of culture conditions.

They prepared the porous Si samples in an electro-chemical etch. The porosity of their porous Si substrates was approximately 70%, with an average pore size of 2–5 nm. The samples were then subjected to oxidizing conditions which generated a thin (~5 nm) oxide layer. Initially, the cells were exposed to a Si oxide surface rather than pure Si; however, FTIR spectroscopy showed that the oxidized porous Si also contained the Si-Si crystalline vibrational mode, indicating that nanocrystalline Si was still present. The oxidized surface was therefore similar to the surface of bioactive glass, which has been shown to be compatible with osteoblasts (ElGhannam et al 1997a, b). Although this treatment rendered the Si surface less electro-active, they found electrical control of the surface could be retained through electron tunneling through the thin oxide layer. AFM images revealed that the nano-topology of the porous Si was relatively unchanged with the addition of cell matrix and adhesion molecules, implicating surface chemistry as the dominant variable. Cells in all conditions remained viable at comparable levels, suggesting that cell viability on nanoporous Si approached that found on a comparative biocompatible standard, tissue culture polystyrene. Their data suggests that there are no gross, long-term (~ weeks) cytotoxic effects of nanoporous Si on primary hepatocytes, despite the harsh electrochemical reaction conditions and high concentrations of HF used in the preparation of the porous Si.

In 2002, Cunin et al (2002) reported a method for optically encoding micrometre-sized nanostructured particles of porous Si. They generated multilayered porous films in crystalline Si using a periodic electrochemical etch. This resulted in photonic crystals with well-resolved and narrow optical reflectivity features. Millions of possible codes could be prepared in this manner. Micrometre-sized particles were then produced by ultrasonic fracture, mechanical grinding or by lithographic means. In order to test the reliability of the encoding approach in a biomolecular screening application, they prepared two different batches of encoded particles as single rugate structures (multilayered stacks in which the refractive index varies sinusoidally, resulting in a mirror with high reflectivity in a narrow spectral region). Both batches of particles were ozone oxidized to improve their stability in aqueous media and to provide a hydrophilic surface. Particles coded with a 750-nm spectral feature were then treated with a concentrated solution of bovine serum albumin (BSA) and incubated for three hours. This batch of particles served as the control.

In a separate Petri dish, 540-nm-encoded particles were exposed to 50 µg/mL rat albumin in buffer, and incubated for two hours. This operation resulted in a specific modification of the surface of the particles by direct adsorption of the protein. The rat-albumin-modified particles were then exposed to a primary rabbit anti-rat-albumin antibody in a concentrated solution of BSA, and incubated for one hour to obtain a specific antibody–antigen interaction. Both batches of particles were then mixed together and incubated for one hour in the presence of FITC (fluorescein isothiocyanate) conjugated goat anti-rabbit immunoglobulin-G in a BSA solution. Detection of analyte binding to the encoded particles was then performed by fluorescence and spectral reflectance microscopy Decoding, performed on 16 particles, yielded the following results: among eight green fluorescent particles, eight particles were positively decoded as belonging to the functionalized rat albumin batch. Among the eight non-luminescent particles, six particles were correctly decoded, one particle displayed the incorrect code and one particle was unreadable.

Perez et al (2003) synthesized nanometric particles from luminescent (red, in approximately 625 nm) porous Si film to later inoculate in *Bacillus subtilis* and *Klebsiella pneumoniae* bacterial strains. They compared the behavior of their growth curve with the ones reported for *Corynebacterium xerosis* and *Escherichia coli*. The *B. subtilis*, as well as the *K. pneumoniae* bacteria growth curves with Si particles present changed compared to the standard curves. The *B. subtilis* growth curve

with nanometric particles of Si grew below the standard curve after the fifth hour, while in the *K. pneumoniae* this happened after the eighth hour. Based on these preliminary findings they speculated that at this point in time a critical population is present, and this may give rise to the possible incorporation of the Si particles by the bacteria. The stationary region, in both cases, took place sooner than in the standard curve. No significant oscillations were observed in any case, which differed from the *C. xerosis* curve where oscillations of intervals of almost one hour were reported. In addition, these curves had a different behavior compared with the *E. coli* growth curve, in which no significant differences between the standard and the particle containing sample were reported. The different and particular behavior that each bacterium presents when grown in a medium containing nanometric Si particles supports the idea that these particles can work well as a bacteriological sensor.

A new commercially available biomaterial, BioSilicon™ (from pSivida), is a nanostructured form of elemental Si, engineered to create a "honeycomb" structure of pores. In pre-clinical studies pSivida has shown that BioSilicon is both biodegradable and biocompatible. Their studies showed that BioSilicon dissolves in body fluids into silicic acid, commonly found in everyday foods. pSivida's core focus is the development of applications for controlled release drug delivery. Other potential applications across the healthcare sector include diagnostics, targeted cancer therapies (including brachytherapy and localized chemotherapy), orthopedics, and tissue engineering.

A recent study of porous Si-based scaffolds for tissue engineering and other biomedical applications by pSiMedica scientists and their colleagues at the Texas Christian University (Coffer et al 2005) demonstrated that highly porous scaffolds composed of mesoporous Si and commonly used biopolymers such as polycaprolactone exhibit an interfacial behavior that promotes calcification in simulated plasma and also sustain the in vitro stability and proliferation of fibroblasts, an active component of connective tissue in implant surfaces. They believe that this type of scaffold presents a new platform relevant to orthopedic tissue engineering with "tunable" properties (mechanical strength, controlled release of useful substances to living tissue, and rate of resorption of the composite to the host surroundings) that can be controlled.

Foraker et al (2003) found that microfabricated porous Si particles enhanced paracellular delivery of insulin across intestinal Caco-2 cell monolayers. The novel porous Si microparticles were fabricated and loaded with FITC-insulin,

a model hydrophilic pharmacologically active protein, along with varied doses of sodium laurate (C12), a well-known permeation enhancer. Particle and liquid formulations were compared as a function of apical to basolateral flux of FITC-insulin across differentiated human intestinal Caco-2 cell monolayers grown on Transwell® inserts. The flux of FITC-insulin from Si particles across cell monolayers was nearly 10-fold higher compared with liquid formulations with permeation enhancer and approximately 50-fold compared with liquid formulations without enhancer. By increasing C12 dose per particle with a concomitant decrease in total particles added per monolayer, the percent of FITC-insulin transport resulted in a linear increase up to 25% monolayer coverage. Although maintaining monolayer integrity and transepithelial electrical resistance, maximum drug transport (20%/h) was achieved with 0.337 μg C12 dose per particle, and total particle loading at 25% monolayer coverage. This study showed that drug permeation rates across Caco-2 cell monolayers could be enhanced significantly using porous Si particles as delivery vehicles. Of particular note, the drug transport efficiency could be augmented at least 10-fold when drug formulations were delivered in porous Si particles compared with liquid formulations, and up to 100-fold compared with formulations without permeation enhancers.

Li and Ruckenstein (2004) used UV-induced graft polymerization of acrylic acid (AAc) on the surface of Si nanoparticles to prepare a stable aqueous luminescent Si nanoparticle solution (see Figure 7). The Si nanoparticles were produced using the method described above by Li et al (2003). By grafting a water-soluble polymer on the particle surface, the dispersions in water of the Si nanoparticles became very stable and clear aqueous solutions could be obtained. XPS and NMR spectroscopy confirmed that PAAc was covalently grafted to the Si nanoparticles. The grafted PAAc on Si particles increased not only the dispersibility but also improved the PL stability of the Si nanoparticles against degradation by water. The surface-modified nanoparticles were used as biological labels for cell imaging. The Si quantum dot labels exhibited bright fluorescence images and provided higher resistance to photobleaching than the commonly used organic dyes.
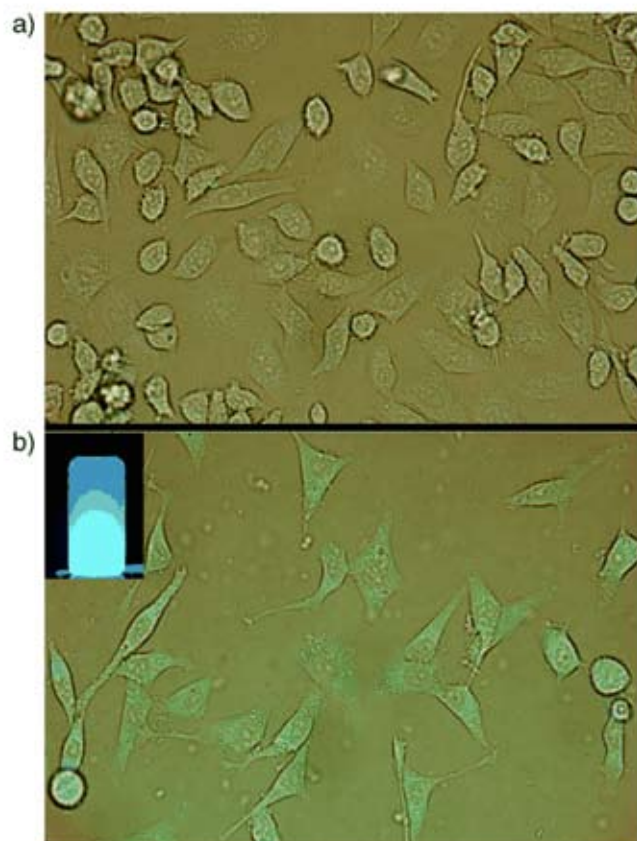
Warner et al (2005) describe a simple room-temperature synthesis for producing water-soluble Si quantum dots that exhibit strong blue PL with a rapid rate of recombination. Silicon quantum dots with a narrow size distribution were synthesized using reverse micelles and powerful hydride reducing agents at room temperature and pressure. The surface of the Si quantum dots was made hydrophilic by modification with allylamine. The Si quantum dots dispersed in an aqueous environment displayed strong PL in the blue region of the visible spectrum, with a 10% quantum yield for the PL. The optical properties of the Si quantum dots displayed features in both the absorption and emission spectra attributed to the direct bandgap transitions in Si quantum dots with a carbon surface termination. Time resolved PL spectroscopy revealed a rapid recombination normally associated with direct bandgap materials. The ease of synthesis and optical
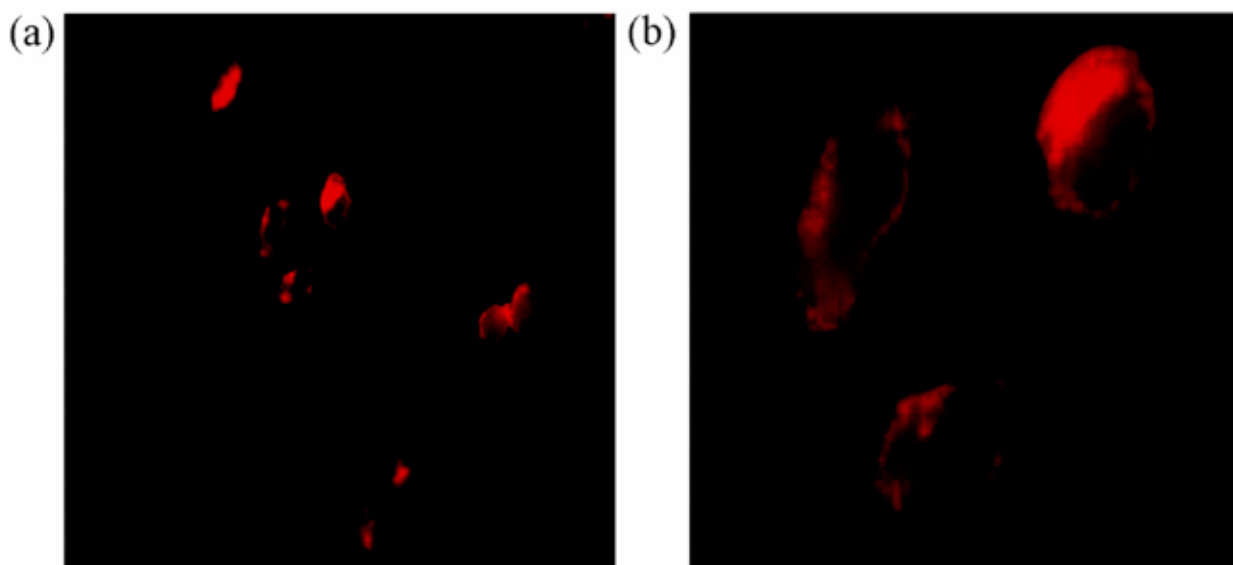
Figure 7 Fluorescent microscopy image of CHO cells labelled with PAAc-Si nanoparticles (b is a higher magnification of a). Reprinted with permission from Li ZF, Ruckenstein E. 2004. Water-soluble poly(acrylic acid) grafted luminescent silicon nanoparticles and their use as fluorescent biological staining labels. *Nano Lett*, 4:1463-7. Copyright © 2005 American Chemical Society.

properties make the Si quantum dots reported by Warner and co-workers excellent candidates for biomedical applications, as demonstrated by the imaging of allylamine-capped Si quantum dots in HeLa cells (Figure 8).

In this experiment, an excitation wavelength of 365 nm was used and the emission at 480 nm was monitored. The control image (Figure 8a) shows minimal fluorescence from the HeLa cells relative to the HeLa cells with the incorporated Si quantum dots (Figure 8b). Thus, the fluorescence observed in the HeLa cells in Figure 8b arises from the emission from Si quantum dots and not autofluorescence from the cells. The inset in the top left corner of Figure 8b shows the bright blue fluorescence from a vial of allylamine-capped Si quantum dots in water when excited with UV light. The bright blue fluorescence from the Si quantum dots is distributed uniformly inside the cytosol of the HeLa cells and this shows the possibility of using these hydrophilic Si quantum dots as chromophores in biological fluorescence imaging.

Conclusions and potential prospects

Silicon nanoparticles are not yet ready for routine use as biological labels. They are, however, a promising technology because of several factors: (i) the robust and flexible surface chemistry of Si facilitates the conjugation of DNA or protein probes by methods of organic chemistry; (ii) red light emission at small particle size; (iii) preliminary indications are that they do not show the same toxicity as heavy-metal chalcogenide based semiconductors; and (iv) they are photostable and have tunable luminescence. In order to increase their utility, the preparation techniques necessary to reliably produce controlled particle sizes with appropriate biochemical functionality (eg, DNA/PNA probes and antibodies) need to be improved. Accurate information on the cytotoxicity of quantum dots (of all kinds) is also necessary even if the particles are to be used only in cultured cells because it is essential to understand the extent to which they perturb the system under study.

Figure 8 Overlay of the transmission and fluorescence microscope images of a) HeLa cells in the absence of any quantum dots and b) HeLa cells with silicon quantum dots incorporated inside the cytosol. Inset: fluorescence from a vial of allylamine-capped silicon quantum dots in water when excited with a UV lamp. Reprinted with permission from Warner JH, Hoshino A, Yamamoto K, et al. 2005. Water-soluble photoluminescent silicon quantum dots. *Angew Chem-Int Edit*, 44:4550-4. Copyright © 2005 WILEY-VCH.

References

Akerman ME, Chan WC, Laakkonen P, et al. 2002. Nanocrystal targeting in vivo. *Proc Natl Acad Sci U S A*, 99:12617-21. Epub 2002 Sep 16.

Alivisatos AP, Gu W, Larabell C. 2005. Quantum Dots as Cellular Probes. *Annu Rev Biomed Eng*, 7:55-76.

Asanuma H, Lopinski GP, Yu HZ. 2005. Kinetic control of the photochemical reactivity of hydrogen-terminated silicon with bifunctional molecules. *Langmuir*, 21:5013-18.

Bakalova R, Ohba H, Zhelev Z, et al. 2004. Quantum dot anti-CD conjugates: Are they potential photosensitizers or potentiators of classical photosensitizing agents in photodynamic therapy of cancer? *Nano Lett*, 4:1567-73.

Bakalova R, Zhelev Z, Ohba H, et al. 2005. Quantum dot-conjugated hybridization probes for preliminary screening of siRNA sequences. *J Am Chem Soc*, 127:11328-35.

Baldwin RK, Pettigrew KA, Ratai E, et al. 2002. Solution reduction synthesis of surface stabilized silicon nanoparticles. *Chem Commun*, 17:1822-3.

Bateman JE, Eagling RD, Worrall DR, et al. 1998. Alkylation of porous silicon by direct reaction with alkenes and alkynes. *Angew Chem-Int Edit*, 37:2683-5.

Belomoin G, Alsalhi M, Al Aql A, et al. 2004. X-ray structure factors for Si nanoparticles. *J Appl Phys*, 95:5019-22.

Belomoin G, Therrien J, Smith A, et al. 2002. Observation of a magic discrete family of ultrabright Si nanoparticles. *Appl Phys Lett*, 80:841-3.

Bley RA, Kauzlarich SM. 1996. A low-temperature solution phase route for the synthesis of silicon nanoclusters. *J Am Chem Soc*, 118:12461-2.

Bley RA, Kauzlarich SM, Davis JE, et al. 1996. Characterization of silicon nanoparticles prepared from porous silicon. *Chem Mat*, 8:1881-8.

Botti S, Terranova ML, Sessa V, et al. 2001. Silicon quantum dots in diamond matrix: a new synthesis route. *Appl Organomet Chem*, 15:388-92.

Brus L. 1994. Luminescence of silicon materials - chains, sheets, nanocrystals, nanowires, microcrystals, and porous silicon. *J Phys Chem*, 98:3575-81.

Buriak JM. 2002. Organometallic chemistry on silicon and germanium surfaces. *Chem Rev*, 102:1271-308.

Canham LT. 1990. Silicon quantum wire array fabrication by electrochemical and chemical dissolution of wafers. *Appl Phys Lett*, 57:1046-8.

Carlisle JA, Germanenko IN, Pithawalla YB, et al. 2001. Morphology, photoluminescence and electronic structure in oxidized silicon nanoclusters. *J Electron Spectrosc Relat Phenom*, 114**:**229-34.

Chan WC, Maxwell DJ, Gao X, et al. 2002. Luminescent quantum dots for multiplexed biological detection and imaging. *Curr Opin Biotechnol*, 13**:**40-6.

Chao Y, Krishnamurthy S, Montalti M, et al. 2005. Reactions and luminescence in passivated Si nanocrystallites induced by vacuum ultraviolet and soft-x-ray photons. *J Appl Phys*, 98**:**044316.

Chin V, Collins BE, Sailor MJ, et al. 2001. Compatibility of primary hepatocytes with oxidized nanoporous silicon. *Adv Mater*, 13**:**1877-80.

Choi BH, Hwang SW, Kim IG, et al. 1998. Fabrication and room-temperature characterization of a silicon self-assembled quantum-dot transistor. *Appl Phys Lett*, 73**:**3129-31.

Cichos F, Martin J, von Borczyskowski, C. 2004. Emission intermittency in silicon nanocrystals. *Phys Rev B*, 70**:**115314-22.

Clapp AR, Medintz IL, Mauro JM, et al. 2004. Fluorescence resonance energy transfer between quantum dot donors and dye-labeled protein acceptors. *J Am Chem Soc*, 126**:**301-10.

Coffer JL, Whitehead MA, Nagesha DK, et al. 2005. Porous silicon-based scaffolds for tissue engineering and other biomedical applications. *Phys Status Solidi A-Appl Mat*, 202**:**1451-5.

Credo GM, Mason MD, Buratto SK. 1999. External quantum efficiency of single porous silicon nanoparticles. *Appl Phys Lett*, 74**:**1978-80.

Cunin F, Schmedake TA, Link JR, et al. 2002. Biomolecular screening with encoded porous-silicon photonic crystals. *Nat Mater*, 1**:**39-41.

Delerue C, Allan G, Lannoo M. 1993. Theoretical Aspects of the Luminescence of Porous Silicon. *Phys Rev B*, 48**:**11024-36.

Derfus AM, Chan WCW, Bhatia SN. 2004. Probing the cytotoxicity of semiconductor quantum dots. *Nano Lett*, 4**:**11-18.

Dick CAJ, Brown DM, Donaldson K, et al. 2003. The role of free radicals in the toxic and inflammatory effects of four different ultrafine particle types. *Inhal Toxicol*, 15**:**39-52.

Ding ZF, Quinn BM, Haram SK, et al. 2002. Electrochemistry and electrogenerated chemiluminescence from silicon nanocrystal quantum dots. *Science*, 296**:**1293-7.

Dinh LN, Chase LL, Balooch M, et al. 1996. Optical properties of passivated Si nanocrystals and SiOx nanostructures. *Phys Rev B*, 54**:**5029-37.

Donaldson K, Stone V, Gilmour PS, et al. 2000. Ultrafine particles: mechanisms of lung injury. *Philos Trans R Soc Lond Ser A-Math Phys Eng Sci*, 358**:**2741-8.

Donaldson K, Stone V, Tran CL, et al. 2004. Nanotoxicology. *Occup Environ Med*, 61**:**727-8.

Dubertret B, Skourides P, Norris DJ, et al. 2002. In vivo imaging of quantum dots encapsulated in phospholipid micelles. *Science*, 298**:**1759-62.

Dwarakanath S, Bruno JG, Shastry A, et al. 2004. Quantum dot-antibody and aptamer conjugates shift fluorescence upon binding bacteria. *Biochem Biophys Res Commun*, 325**:**739-43.

Ebenstein Y, Mokari T, Banin, U. 2004. Quantum-dot-functionalized scanning probes for fluorescence-energy-transfer-based microscopy. *J Phys Chem B*, 108**:**93-9.

Efros AL, Rosen M. 1997. Random telegraph signal in the photoluminescence intensity of a single quantum dot. *Phys Rev Lett*, 78**:**1110-13.

ElGhannam A, Ducheyne P, Shapiro IM. 1997a. Formation of surface reaction products on bioactive glass and their effects on the expression of the osteoblastic phenotype and the deposition of mineralized extracellular matrix. *Biomaterials*, 18**:**295-303.

ElGhannam A, Ducheyne P, Shapiro IM. 1997b. Porous bioactive glass and hydroxyapatite ceramic affect bone cell function in vitro along different time lines. *J Biomed Mater Res*, 36**:**167-80.

English DS, Pell LE, Yu ZH, et al. 2002. Size tunable visible luminescence from individual organic monolayer stabilized silicon nanocrystal quantum dots. *Nano Lett*, 2**:**681-5.

Fojtik A, Henglein A. 1994. Luminescent colloidal silicon particles. *Chem Phys Lett*, 221**:**363-7.

Foraker AB, Walczak RJ, Cohen MH, et al. 2003. Microfabricated porous silicon particles enhance paracellular delivery of insulin across intestinal Caco-2 cell monolayers. *Pharm Res*, 20**:**110-16.

Fu AH, Gu WW, Larabell C, et al. 2005. Semiconductor nanocrystals for biological imaging. *Curr Opin Neurobiol*, 15**:**568-75.

Furukawa S, Miyasato T. 1988. Quantum Size Effects on the Optical Band-Gap of Microcrystalline Si-H. *Phys Rev B*, 38**:**5726-9.

Garoufalis CS, Zdetsis D, Grimme S. 2001. High level ab initio calculations of the optical gap of small silicon quantum dots. *Phys Rev Lett*, 87.

Germanenko IN, Dongol M, Pithawalla YB, et al. 2000. Effect of atmospheric oxidation on the electronic and photoluminescence properties of silicon nanocrystals. *Pure Appl Chem*, 72**:**245-55.

Giesen B, Wiggers H, Kowalik A, et al. 2005. Formation of Si-nanoparticles in a microwave reactor: Comparison between experiments and modelling. *J Nanopart Res*, 7**:**29-41.

Green M, Howman E. 2005. Semiconductor quantum dots and free radical induced DNA nicking. *Chem Commun*, 121-3.

Hata K, Yoshida S, Fujita M, et al. 2001. Self-assembled monolayer as a template to deposit silicon nanoparticles fabricated by laser ablation. *J Phys Chem B*, 105**:**10842-6.

Heinrich JL, Curtis CL, Credo GM, et al. 1992. Luminescent colloidal silicon suspensions from porous silicon. *Science*, 255**:**66-8.

Holmes JD, Ziegler KJ, Doty RC, et al. 2001. Highly luminescent silicon nanocrystals with discrete optical transitions. *J Am Chem Soc*, 123**:**3743-8.

Hoshino A, Fujioka K, Oku T, et al. 2004. Physicochemical properties and cellular toxicity of nanocrystal quantum dots depend on their surface modification. *Nano Lett*, 4**:**2163-9.

Howarth M, Takao K, Hayashi Y, et al. 2005. Targeting quantum dots to surface proteins in living cells with biotin ligase. *Proc Natl Acad Sci U S A*, 102**:**7583-8. Epub 2005 May 16.

Hua FJ, Swihart MT, Ruckenstein E. 2005. Efficient surface grafting of luminescent silicon quantum dots by photoinitiated hydrosilylation. *Langmuir*, 21**:**6054-62.

Invitrogen 2005. The handbook - a guide to fluorescent probes and labeling technologies. Invitrogen Corp.

Itoh C, Tanimura K, Itoh N, et al. 1989. Threshold Energy for Photogeneration of Self-Trapped Excitons in Sio2. *Phys Rev B*, 39**:**11183-6.

Jaiswal JK, Mattoussi H, Mauro JM, et al. 2003. Long-term multiple color imaging of live cells using quantum dot bioconjugates. *Nat Biotechnol*, 21**:**47-51. Epub 2002 Dec 2.

Jaiswal JK, Simon SM. 2004. Potentials and pitfalls of fluorescent quantum dots for biological imaging. *Trends Cell Biol*, 14**:**497-504.

Jang H, Pell LE, Korgel BA, et al. 2003. Photoluminescence quenching of silicon nanoparticles in phospholipid vesicle bilayers. *J Photochem Photobiol A-Chem*, 158**:**111-17.

Kapaklis V, Politis C, Poulopoulos P, et al. 2005. Photoluminescence from silicon nanoparticles prepared from bulk amorphous silicon monoxide by the disproportionation reaction. *Appl Phys Lett*, 87**:**123114-16.

Kirchner C, Liedl T, Kudera S, et al. 2005. Cytotoxicity of colloidal CdSe and CdSe/ZnS nanoparticles. *Nano Lett*, 5**:**331-8.

Kirkey WD, Sahoo Y, Li XG, et al. 2005. Quasi-reversible photoluminescence quenching of stable dispersions of silicon nanoparticles. *J Mater Chem*, 15**:**2028-34.

Kohno H, Takeda S. 1998. Self-organized chain of crystalline-silicon nanospheres. *Appl Phys Lett*, 73**:**3144-6.

Kondoh M, Araragi S, Sato K, et al. 2002. Cadmium induces apoptosis partly via caspase-9 activation in HL-60 cells. *Toxicology*, 170**:**111-17.

Kovalev D, Heckler H, Ben-Chorin M, et al. 1998. Breakdown of the k-conservation rule in Si nanocrystals. *Phys Rev Lett*, 81**:**2803-6.

Lauerhaas JM, Credo GM, Heinrich JL, et al. 1992. Reversible Luminescence Quenching of Porous Si by Solvents. *J Am Chem Soc*, 114**:**1911-12.

Ledoux G, Gong J, Huisken F, et al. 2002. Photoluminescence of size-separated silicon nanocrystals: Confirmation of quantum confinement. *Appl Phys Lett*, 80**:**4834-6.

Lee S, Cho WJ, Chin CS, et al. 2004. Optical properties of silicon nanoparticles by ultrasound-induced solution method. *Jpn J Appl Phys Part 2 - Lett Express Lett*, 43:L784-L6.

Li XG, He YQ, Swihart MT. 2004a. Surface functionalization of silicon nanoparticles produced by laser-driven pyrolysis of silane followed by HF-HNO3 etching. *Langmuir*, 20:4720-7.

Li XG, He YQ, Talukdar SS, et al. 2003. Process for preparing macroscopic quantities of brightly photoluminescent silicon nanoparticles with emission spanning the visible spectrum. *Langmuir*, 19:8490-6.

Li ZF, Ruckenstein E. 2004. Water-soluble poly(acrylic acid) grafted luminescent silicon nanoparticles and their use as fluorescent biological staining labels. *Nano Lett*, 4:1463-7.

Li ZF, Swihart MT, Ruckenstein E. 2004b. Luminescent silicon nanoparticles capped by conductive polyaniline through the self-assembly method. *Langmuir*, 20:1963-71.

Lie LH, Duerdin M, Tuite EM, et al. 2002a. Preparation and characterisation of luminescent alkylated-silicon quantum dots. *J Electroanal Chem*, 538-539:183-90.

Lie LH, Patole SN, Hart ER, et al. 2002b. Photochemical reaction of diazomethane with hydrogen-terminated silicon surfaces. *J Phys Chem B*, 106:113-20.

Lie LH, Patole SN, Pike AR, et al. 2004. Immobilisation and synthesis of DNA on Si(111), nanocrystalline porous silicon and silicon nanoparticles. *Faraday Discuss*, 125:235-49.

Littau KA, Szajowski PJ, Muller AJ, et al. 1993. A luminescent silicon nanocrystal colloid via a high-temperature aerosol reaction. *J Phys Chem*, 97:1224-30.

Liu Q, Kauzlarich SM, 2002. A new synthetic route for the synthesis of hydrogen terminated silicon nanoparticles. *Mater Sci Eng B-Solid State Mater Adv Technol*, 96:72-5.

Liu SM, Sato S, Kimura K. 2005. Synthesis of luminescent silicon nanopowders redispersible to various solvents. *Langmuir*, 21:6324-9.

Liu WL, Zhang M, Lin CL, et al. 2001. Intense blue-light emission from carbon-plasma-implanted porous silicon. *Appl Phys Lett*, 78:37-9.

Mangolini L, Thimsen E, Kortshagen U. 2005. High-yield plasma synthesis of luminescent silicon nanocrystals. *Nano Lett*, 5:655-9.

Mayeri D, Phillips BL, Augustine MP, et al. 2001. NMR study of the synthesis of alkyl-terminated silicon nanoparticles from the reaction of SiCl4 with the zintl salt, NaSi. *Chem Mat*, 13:765-70.

Michalet X, Pinaud FF, Bentolila LA, et al. 2005. Quantum dots for live cells, in vivo imaging, and diagnostics. *Science*, 307:538-44.

Parak WJ, Gerion D, Pellegrino T, et al. 2003. Biological applications of colloidal nanocrystals. *Nanotechnology*, 14:R15-R27.

Parak WJ, Pellegrino T. Plank C. 2005. Labelling of cells with quantum dots. *Nanotechnology*, 16:R9-R25.

Perez L, Flores M, Avalos J, et al. 2003. In Materials Research Society Symposium Proceedings, 737. Materials Research Society.

Pike AR, Lie LH, Eagling RA, et al. 2002. DNA on silicon devices: On-chip synthesis, hybridization, and charge transfer. *Angew Chem-Int Edit*, 41:615-+.

Puzder A, Williamson AJ, Grossman JC, et al. 2003. Computational studies of the optical emission of silicon nanocrystals. *J Am Chem Soc*, 125:2786-91.

Reboredo FA, Galli G, 2005. Theory of alkyl-terminated silicon quantum dots. *J Phys Chem B*, 109:1072-8.

Reboredo FA, Pizzagalli L, Galli G. 2004. Computational engineering of the stability and optical gaps of SiC quantum dots. *Nano Lett*, 4:801-4.

Reddy MP, Hanna NB, Farooqui F. 1997. Ultrafast cleavage and deprotection of oligonucleotides synthesis and use of C-Ac derivatives. *Nucleosides Nucleotides*, 16:1589-98.

Rikans LE, Yamano T. 2000. Mechanisms of cadmium-mediated acute hepatotoxicity. *J Biochem Mol Toxicol*, 14:110-17.

Samia ACS, Chen XB, Burda C. 2003. Semiconductor quantum dots for photodynamic therapy. *J Am Chem Soc*, 125:15736-7.

Sankaran RM, Holunga D, Flagan RC, et al. 2005. Synthesis of blue luminescent Si nanoparticles using atmospheric-pressure microdischarges. *Nano Lett*, 5:537-41.

Schoenfeld O, Zhao X, Christen J, et al. 1996. Formation of Si quantum dots in nanocrystalline silicon. *Solid-State Electronics*, 40:605-8.

Sham TK, Naftel SJ, Kim PSG, et al. 2004. Electronic structure and optical properties of silicon nanowires: A study using x-ray excited optical luminescence and x-ray emission spectroscopy. *Phys Rev B*, 70:045313.

Shen HM, Yang CF, Ong CN. 1999. Sodium selenite-induced oxidative stress and apoptosis in human hepatoma HepG(2) cells. *Int J Cancer*, 81:820-8.

Shiohara A, Hoshino A, Hanaki K, et al. 2004. On the cyto-toxicity caused by quantum dots. *Microbiol Immunol*, 48:669-75.

Sweryda-Krawiec B, Cassagneau T, Fendler JH. 1999. Surface modification of silicon nanocrystallites by alcohols. *J Phys Chem B*, 103:9524-9.

Sychugov I, Juhasz R, Valenta J, et al. 2005. Narrow luminescence linewidth of a silicon quantum dot. *Phys Rev Lett*, 94.

Tang J, Marcus RA. 2005. Diffusion-controlled electron transfer processes and power-law statistics of fluorescence intermittency of nanoparticles. *Phys Rev Lett*, 95:107401.

Tilley RD, Warner JH, Yamamoto K, et al. 2005. Micro-emulsion synthesis of monodisperse surface stabilized silicon nanocrystals. *Chem Commun*, 1833-5.

Valenta J, Janda P, Dohnalova K, et al. 2005. Colloidal suspensions of silicon nanocrystals: from single nanocrystals to photonic structures. *Opt Mater*, 27:1046-9.

van Buuren T, Dinh LN, Chase LL, et al. 1998. Changes in the electronic properties of Si nanocrystals as a function of particle size. *Phys Rev Lett*, 80:3803-6.

Voura EB, Jaiswal JK, Mattoussi H, et al. 2004. Tracking metastatic tumor cell extravasation with quantum dot nanocrystals and fluorescence emission-scanning microscopy. *Nat Med*, 10:993-8. Epub 2004 Aug 29.

Wang L, Reipa V, Blasic J. 2004. Silicon nanoparticles as a luminescent label to DNA. *Bioconjugate Chem*, 15:409-12.

Warner JH, Hoshino A, Yamamoto K, et al. 2005. Water-soluble photoluminescent silicon quantum dots. *Angew Chem-Int Edit*, 44:4550-4.

Wilcoxon JP, Samara GA, Provencio PN. 1999. Optical and electronic properties of Si nanoclusters synthesized in inverse micelles. *Phys Rev B*, 60:2704-14.

Wilson MR, Lightbody JH, Donaldson K, et al. 2002. Interactions between ultrafine particles and transition metals in vivo and in vitro. *Toxicol Appl Pharmacol*, 184:172-9.

Wolkin MV, Jorne J, Fauchet PM, et al. 1999. Electronic states and luminescence in porous silicon quantum dots: The role of oxygen. *Phys Rev Lett*, 82:197-200.

Wu X, Liu H, Liu J, et al. 2003. Immunofluorescent labeling of cancer marker Her2 and other cellular targets with semiconductor quantum dots. *Nat Biotechnol*, 21:41-6. Epub 2002 Dec 2.

Yang CS, Bley RA, Kauzlarich SM, et al. 1999. Synthesis of alkyl-terminated silicon nanoclusters by a solution route. *J Am Chem Soc*, 121:5191-5.

Zhang LB, Coffer JL, Zerda TW, 1998. Properties of luminescent Si nanoparticles in sol-gel matrices. *J Sol-Gel Sci Technol*, 11:267-2.

Zhou ZY, Brus L, Friesner R. 2003. Electronic structure and luminescence of 1.1-and 1.4-nm silicon nanocrystals: Oxide shell versus hydrogen passivation. *Nano Lett*, 3:163-7.

Zou J, Baldwin RK, Pettigrew KA, et al. 2004. Solution synthesis of ultrastable luminescent siloxane-coated silicon nanoparticles. *Nano Lett*, 4:1181-6.